Article

Mechanistic Studies of the Streptomyces bingchenggensis Aldolase-Dehydratase: Implications for Substrate and Reaction Specificity in the Acetoacetate Decarboxylase-Like Superfamily

Lisa Mydy, Robert William Hoppe, Trevor M. Hagemann, Alan W. Schwabacher, and Nicholas Silvaggi

Biochemistry, **Just Accepted Manuscript** • DOI: 10.1021/acs.biochem.9b00652 • Publication Date (Web): 16 Sep 2019

Mechanistic Studies of the *Streptomyces bingchenggensis* Aldolase-Dehydratase: Implications for Substrate and Reaction Specificity in the Acetoacetate Decarboxylase-Like Superfamily

Lisa S. Mydy[a], Robert W. Hoppe[a], Trevor M. Hagemann[a], Alan W. Schwabacher[a], and Nicholas R. Silvaggi[a]*

[a]Department of Chemistry and Biochemistry, University of Wisconsin-Milwaukee, 3210 North Cramer Street, Milwaukee, WI 53211 (USA).

KEYWORDS: aldolase, acetoacetate decarboxylase-like superfamily, enzyme structure and function.

ABSTRACT: The acetoacetate decarboxylase-like superfamily (ADCSF) is a little-explored group of enzymes that may contain new biocatalysts. The low sequence identity (~20%) between many ADCSF enzymes and the confirmed acetoacetate decarboxylases led us to investigate the degree of diversity in reaction and substrate specificity of ADCSF enzymes. We have previously reported on Sbi00515, which belongs to Family V of the ADCSF, and functions as an aldolase-dehydratase. Here, we more thoroughly characterize the substrate specificity of Sbi00515, and find that aromatic, unsaturated aldehydes yield lower K_M and higher k_{cat} values compared to other small electrophilic substrates in the condensation reaction. The roles of several active site residues were explored by site directed mutagenesis and steady state kinetics. The lysine-glutamate catalytic dyad, conserved throughout the ADCSF, is required for catalysis. Tyrosine 252, which is unique to Sbi00515, is hypothesized to orient the incoming aldehyde in the condensation reaction. Transient-state kinetics and an intermediate-bound crystal structure aid in completing a proposed mechanism for Sbi00515.

Introduction

The enzyme Sbi00515 from *Streptomyces bingchenggensis* (UniProt accession ID D7C0E5) belongs to the acetoacetate decarboxylase-like superfamily (ADCSF), however it is not a decarboxylase as the majority of ADCSF enzymes are[1]. Instead, Sbi00515 was shown to be an aldolase-dehydratase capable of condensing pyruvate with a variety of aldehyde substrates, and subsequently dehydrating the resulting C-C bond[1]. This activity prompted us to propose renaming Sbi00515 to SbAD (*S. bingchenggensis* Aldolase-Dehydratase), and it will be referred to thus herein. Other non-decarboxylating ADCSF enzymes have been described, such as MppR from *Streptomyces hygroscopicus*[2] and Swit_4259 from *Sphingomonas wittichii*[3]. The former participates in the biosynthesis of the non-proteinogenic amino acid L-enduracididine by catalyzing the cyclization of 4-hyroxy-2-ketoarginine to give 2-ketoenduracididine. The latter, Swit_4259, has been shown to catalyze the same aldol condensation and dehydration reaction as SbAD, though much less efficiently. The genomic context suggests that Swit_4259 operates within the catabolic pathway of an as-yet-unidentified aromatic hydrocarbon. The weak enzymatic activity observed is likely because Swit_4259 possesses a substrate specificity

profile different from that of SbAD. The biological context of SbAD's enzymatic activity remains obscure.

In our first report on SbAD, we characterized the aldolase-dehydratase activity and compared the structure, with and without pyruvate bound, to both confirmed acetoacetate decarboxylase and MppR. With respect to the enzymatic activity of SbAD, we showed that, while the first activity observed was the aldol cleavage of benzylidene-pyruvate (**1**, Scheme 1a) to benzaldehyde (**2**) and pyruvate (**3**), the enzyme is a more efficient catalyst of the aldol condensation of pyruvate with a number of aldehyde substrates. The best among the aldehydes tested was 3-(2-furyl)acrolein (**4**, Scheme 1b), with k_{cat} = 22.9 ± 0.8 s^{-1} and K_M = 1.2 ± 0.1 mM (k_{cat}/K_M = 1.9 ± 0.17 x 10^4 $M^{-1}s^{-1}$). For comparison, the steady state kinetic parameters for the reaction with **1** were k_{cat} = 1.2 ± 0.2 s^{-1} and K_M = 22.3 ± 7.0 mM (k_{cat}/K_M = 54 ± 19 $M^{-1}s^{-1}$) [1].

Scheme 1. Reactions catalyzed by SbAD.

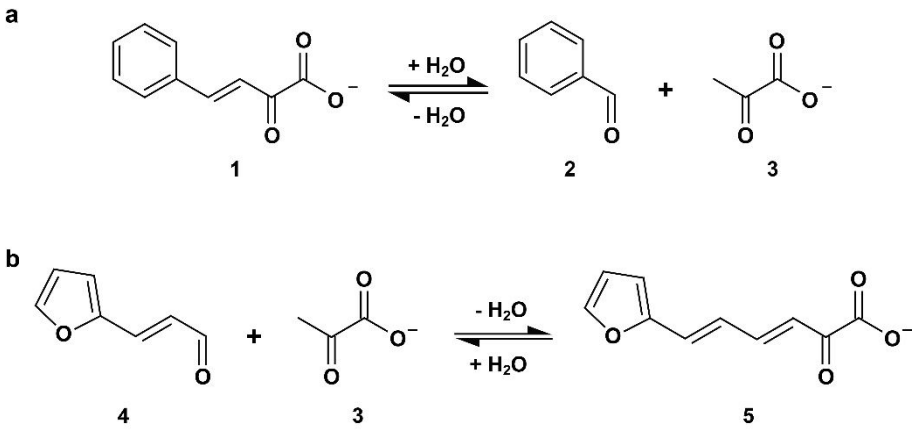

The tertiary structure of SbAD is nearly identical to those of other non-decarboxylating ADCSF enzymes like MppR and Swit_4259, and is remarkably similar to those of the confirmed acetoacetate decarboxylases. The active site architectures of the MppR-like class of ADCSF enzymes are, however, markedly different from those of the decarboxylases that comprise the largest single group within the superfamily. Figure 1 shows an overlay of the active sites of all four of these ADSCF enzymes. The overlay includes the pyruvate (PYR)-bound form of SbAD and the acetyl acetone (PNH)-bound form of *Chromobacterium violaceum* acetoacetate decarboxylase (CvADC)[4]. The most obvious difference between the active sites of these two classes of ADCSF enzymes is the presence of a carboxylate-binding site in the MppR-like proteins. This highly polar

binding site is located close to the catalytic lysine residue common to all ADCSF enzymes and consists of an arginine and a glutamine residue (R114 and Q118 in SbAD). In fact, the motif RGxx[Q/N]xxPKxxG appears to be diagnostic for the MppR-like ADCSF members. The RGxxQ portion of this motif corresponds to the carboxylate-binding site, and the K is the catalytic lysine residue (K122 in SbAD). Interestingly, the three MppR-like enzymes that have been studied thus far exhibit subtle differences in the carboxylate-binding site. In MppR from *Streptomyces hygroscopicus* (ShMppR), the carboxylate-binding site is arranged such that the carboxylate groups of bound α-keto acids (Schiff-base intermediates) are perpendicular to the Cα-Cβ bond[2]. In the carboxylate-binding site of Swit4259, the glutamine residue is replaced by asparagine, which disorders the binding site and appears to destabilize the Schiff base intermediate. This may account, in part, for the apparent catabolic activity of this enzyme[3]. The carboxylate-binding site of SbAD includes a tyrosine, Y24, that alters the orientation of the substrate carboxylate so that it is nearly co-planar with the Cα-Cβ bond. It was proposed that the substrate carboxylate may assist in the aldol chemistry of SbAD[1].

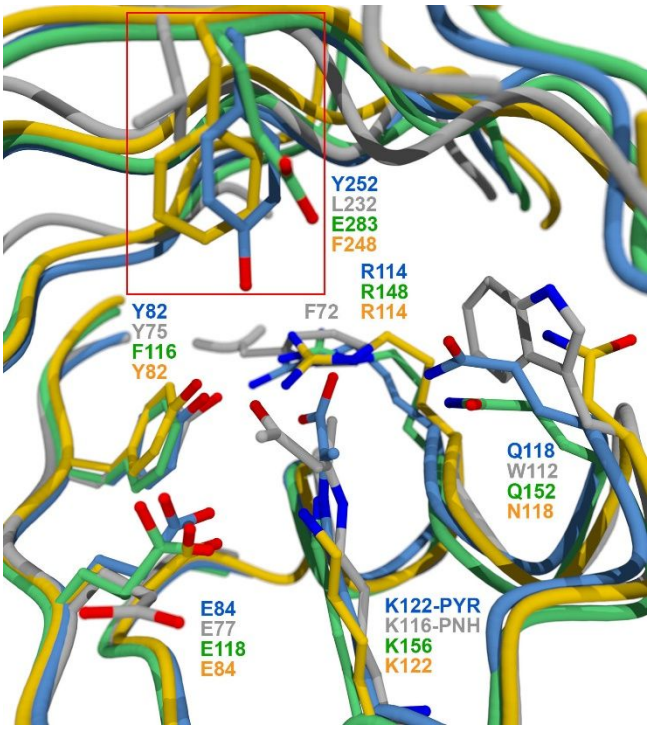

Figure 1. The active sites of four ADCSF enzymes are overlayed in order to highlight the similarities and differences in their active site architectures. The Schiff base complex between SbAD K122 and pyruvate is shown in blue (PDB ID 4ZBT). The analogous complex between the confirmed acetoacetate decarboxylase CvADC K116 and the substrate analog acetylacetate is shown in grey (PDB ID 3BH3). The unliganded structures of MppR (PDB ID 4JM3) and Swit_4259 (PDB ID 5UPB) are shown in green and yellow, respectively. Notice that the acetyl group of acetylacetone, which takes the place of the carboxylate of acetoacetate, points in the opposite direction from the carboxylate group of pyruvate. This is primarily due to the carboxylate-binding site formed

by R114 and Q118 (SbAD numbering) in the MppR-like ADCSF enzymes. This subsite of the active site distinguishes the MppR-like enzymes from the *bona fide* acetoacetate decarboxylases. The position occupied by Y252 in SbAD (red box) constitutes one of the main differences between the active sites of enzymes within the MppR-like family of the ADCSF, such as SbAD, MppR, and Swit_4259.

Another feature of the MppR-like active sites that distinguishes these enzymes from the confirmed acetoacetate decarboxylases and from one another is the identity of the amino acid at position 252 (SbAD numbering). In the acetoacetate decarboxylases, this region of the active site is hydrophobic. For example, the residue at this position is L232 in the prototypical CvADC. In ShMppR, this position in the active site is occupied by E283. The crystal structure with 2-ketoarginine bound suggests that E283 serves to orient the guanidinium group of the substrate for attack at Cγ to form the iminoimidazolidine ring of enduracididine[2]. The positively charged R249 in the Swit_4259 active site and its distance from the catalytic lysine residue led to the proposal that the true substrate of this enzyme is a 7-carbon dicarboxylic acid[3]. Finally, Y252 in the SbAD active site is thought to orient the aldehyde substrate for attack by the Schiff-base enamine in the aldol condensation

reaction, and by extension, to orient water for attack in the retro-aldol cleavage reaction[1]. Other potentially significant residues identified in the SbAD active site are E84, which is conserved in all the ADCSF enzymes identified thus far, and Y82, which is often substituted with phenylalanine. Both of these residues were put forth as possible candidates for the general acid/base catalyst that promotes formation of the enamine with pyruvate.

Herein we present a more elaborate substrate specificity profile of SbAD, together with steady state characterization of active site variants to probe the roles of these residues in substrate binding and catalysis. An intermediate-bound structure and pre-steady state kinetics aid in understanding the chemistry of SbAD and allow us to propose a plausible mechanism for the SbAD-catalyzed aldol condensation reaction.

Materials and Methods

Expression and purification of SbAD. SbAD was expressed and purified as described previously[1]. Briefly, 1L portions of Luria-Bertani medium were inoculated with overnight cultures of BL21 Star (DE3) *E. coli* cells carrying the pE-SUMO-SbAD plasmid and grown at 37°C with shaking at 250 rpm. When cultures reached an OD_{600nm} of approximately 0.8, expression was induced with 0.4 mM IPTG, the temperature was reduced to 25 °C, and the cultures were grown for an additional 16 h at 250 rpm. Cells were harvested by centrifugation, resuspended in 5 mL/g of buffer A (25 mM Tris pH 8.0, 300 mM NaCl, 10 mM imidazole), supplemented with 1 mg/mL lysozyme and frozen overnight at -20°C. Cells were lysed by thawing at room temperature for 2 h, after which DNase I was added, and the lysate was clarified by centrifugation for 45 min at 39,000 x g and 4 °C. The clarified lysate was filtered and applied to a 5 mL HisTrap column (GE Life Sciences). The protein was eluted with buffer B (25 mM Tris pH 8.0, 300 mM NaCl, 250 mM imidazole) in a four-step gradient. The fractions with significant absorbance at 280 nm were analyzed by polyacrylamide gel electrophoresis and those containing the His_6-SUMO-SbAD fusion protein were pooled in SnakeSkin dialysis tubing (3500 MWCO;

Thermo Scientific), SUMO protease was added to a final concentration of ~3 μM, and dialyzed overnight against 3.5 L of 25 mM Tris pH 8.0, 150 mM NaCl. The dialysate was passed through the same HisTrap column a second time to remove the cleaved His_6-SUMO tag and the protease.

Site-directed mutagenesis and preparation of SbAD variants. Primers appropriate for each mutation were synthesized by Integrated DNA Technologies, Inc (see Table S1). The PCR was based on the QuikChange site-directed mutagenesis kit (Agilent). Mutants were confirmed by sequencing before transformation of the mutagenic plasmid to BL21 Star (DE3) *E. coli* cells (Invitrogen). Mutants of SbAD were expressed and purified in the same manner as WT SbAD. A fresh 5 mL HisTrap column was used to purify each variant.

*Preparation of cinnamylidenepyruvate (**29**)*. The synthesis of **29**, potassium (3E,5E)-2-oxo-6-phenylhexa-3,5-dienoate proceeded by dissolving cinnamaldehyde (3.29g, 25 mmol), sodium pyruvate (2.80g, 25 mmol), and sodium hydroxide (0.112g, 2.8 mmol) in 25 mL of methanol and heating at reflux for 17 h under N_2. Then sodium hydroxide

(0.403g, 10.0 mmol) in 50 mL of methanol was added and reflux was continued for 3 h. After cooling the yellow solid was collected via vacuum filtration, washed with methanol, and dried under vacuum. The solid was then dissolved in 185 mL of 2.4 M triethylammonium bicarbonate and extracted with 200 mL portions of dichloromethane. The organics were combined, dried over magnesium sulfate and concentrated to afford an auburn oil. The oil was dissolved in 50 mL of ethyl acetate to which potassium 2-ethylhexanoate (0.807g, 4.4 mmol) was added forming an immediate precipitate. The solid was collected via centrifugation and recrystallized from methanol:ethyl acetate. 0.914g (15% yield) of yellow solid **29** was obtained with 99.4% purity, 0.6% by mass pyruvate. ^{1}H NMR (see Figure S1) (300MHz, D_2O): δ7.63 (d, 2H, J=8.1Hz); δ7.51 (q_{AB}, 1H, J=15.6Hz, 9.6Hz); δ7.48-7.41(m,3H); δ7.20-7.07 (m,2H, J=15.6Hz, 8.7Hz)); δ6.40 (d, 1H, J=15.6Hz) ^{13}C NMR (300MHz, D_2O): δ 198.9; δ 173.6; δ 150.9; δ 149.0; δ 144.1; δ 142.4; δ 132.3; δ 129.9; δ 129.0; δ 125.8.

*Preparation of 4-nitrocinnamylidenepyruvate (**30**)*. The synthesis of potassium (3E,5E)-6-(4-nitrophenyl)-2-oxohexa-3,5-dienoate, **30**, proceded by dissolving 4-nitrocinnamaldehyde (1.46g, 8.2 mmol), sodium pyruvate (1.35g, 12.28 mmol), and sodium hydroxide (0.113g, 2.8 mmol) in 35 mL of methanol and heating to reflux under N_2. After 3.5 h the reaction was cooled, concentrated, and dried under vacuum overnight. The crude solid was dissolved into 240 mL of 2.4 M triethylammonium bicarbonate and extracted with 600 mL of dichloromethane. The organics were combined, dried over magnesium sulfate and concentrated. The solid was then dissolved in 140 mL of ethyl acetate and the product precipitated with potassium 2-ethylhexanoate (1.36g, 7.4 mmol) in 50 mL of ethyl acetate. The precipitate was collected via centrifugation, washed with ethyl acetate and recrystallized from methanol:ethyl acetate. 0.1257g (5% yield) of **30** was obtained with 98.0% purity and 2.0% pyruvate by mass. ^{1}H NMR (see Figure S2) (300MHz, D_2O): δ8.21 (d, 2H, J=8.4Hz); δ7.72 (d, 2H, J=8.7Hz); δ7.46 (q_{AB}, 1H, J=15.3Hz, 8.4Hz); δ7.20 (m, 2H); δ6.46 (d, 2H, J=15.6Hz) ^{13}C NMR (300MHz, D_2O): δ 198.9; δ 173.6; δ 150.9; δ 149.0; δ 144.1; δ 142.4; δ 132.3; δ 129.9; δ 129.0; δ 125.8.

Steady state kinetic analysis. The extinction coefficients of the various products of SbAD were determined as previously described[1]. All reactions were done in triplicate at 25 °C in 50 mM Bis-Tris pH 6.5 on a TgK Scientific SF-61DX2 stopped flow instrument, unless otherwise stated. The initial velocity of SbAD-catalyzed condensation of pyruvate with the various aldehydes tested was measured directly by monitoring the increase of absorbance at the optimal wavelength for each dienone product. Optimal wavelengths for observing the reactions and the relevant extinction coefficients are listed in Table 1. The substrates **6-14** in Scheme 2 and compounds **15-25** in Scheme 3 contained ≤ 5% acetonitrile in their final reaction volume to maintain solubility. The k_{cat} and apparent K_M values were determined by fitting the initial velocity data using the equation $v_0 = V_{max}[A]/(K_M+[A])$, where V_0 is the initial velocity, V_{max} is the maximal velocity, and [A] is the concentration of aldehyde, cinnamylidenepyruvate (Scheme 4, **29**), or 4-nitrocinnamylidenepyruvate (Scheme 4, **30**), and K_M is the Michaelis constant.

High-Performance Liquid Chromatography Analysis of SbAD Reaction Mixtures. The detection of SbAD substrates and products at 330 nm used the same column and gradient

as previously described[1]. Briefly, the stationary phase was a 50 mm x 2.0 mm, 2.5 µm Synergy Polar RP column (Phenomenex), and the starting mobile phase was 80% buffer A (0.1% trifluoroacetic acid/water) and 20% buffer B (0.1% trifluoroacetic acid/acetonitrile). The analytes were separated over a gradient from 20-50% buffer B over 17 min using an Agilent 1220 HPLC system. Reaction mixtures were 1 mL; substrates and standards were all 1 mM in 100 mM MOPS pH 7.0. Reactions contained 1 µM SbAD.

Fluorescence Titration. Binding constants were measured by fluorescence titration using a Hitachi F-4500 fluorimeter. SbAD (1 µM) in 50 mM Bis-Tris pH 6.5 was titrated with substrate. The intrinsic tryptophan fluorescence was excited at 280 nm and monitored by scanning the emission wavelength from 300-600 nm. The fluorescence intensity with no ligand present was taken as 0% fractional saturation. This value was used to convert fluorescence intensities in the presence of ligand to fractional saturation. All fluorescence measurements were done in triplicate. A plot of fractional saturation versus ligand concentration was fitted in Origin 2015 (OriginLab) against the equation Y

= [A]/(K_D+[A]), where Y is fractional saturation, [A] is the concentration of ligand, and K_D is the dissociation constant.

Pre-Steady state kinetic analysis. Transient state data were collected on a TgK Scientific SF-61DX2 stopped flow instrument in single mixing mode. Single turnover experiments were performed by mixing 200 μM wild-type SbAD in 50 mM Bis-Tris pH 6.5 with 40 μM **30** in the same buffer (100 μM and 20 μM, respectively after mixing). Absorbance data were recorded for 1s at single wavelengths between 300 and 450 nm at 5 nm intervals. The observed transients at 350 and 415 nm were fit to a single exponential ($y = A(e^{-kt}) + C$) where A is the amplitude of the absorbance change, k is the observed rate constant, t is time, and C is the absorbance at infinite time. Multiple turnover experiments were performed at various limiting concentrations of wild-type SbAD and saturating amounts of pyruvate and cinnamaldehyde (**7**). The enzyme, serially diluted to 2.5, 5.0, or 10.0 μM in 50 mM Bis-Tris pH 6.5 was mixed with 200 mM pyruvate, 2.5 mM cinnamaldehyde, 5 % acetonitrile in the same buffer (1.25, 2.5, or 5.0

μM enzyme, 100 mM pyruvate, and 1.25 mM **7** after mixing). The absorbance at 430 nm was monitored for 5-10s. The data fit well to a single exponential followed by steady state turnover ($y = A(e^{-kt}) + mt + C$), where A is the amplitude of the exponential portion, k is the observed rate constant, t is time, m is the steady state rate (absorbance s^{-1}), and C is the absorbance at the end of the exponential phase.

Crystallization and structure determination. Structure determination of $SbAD^{Y252F}$ proceeded in a similar manner to that of SbAD WT[1]. Briefly, $SbAD^{Y252F}$ crystallized in 3.5-4.0 M potassium formate, 2-5% polyethylene glycol monomethyl ether 2000 (PEG MME 2000), and 100 mM Bis-Tris propane pH 9.0 at room temperature by the hanging drop vapor diffusion method. Drops consisted of 1-2 μL of 45 mg/mL $SbAD^{Y252F}$ and 1 μL crystallization solution. Plate-shaped crystals grew in 3-4 days. Crystals were transferred to a soaking solution of 4.0 M potassium formate, 3 % PEG MME 2000, 100 mM Bis-Tris propane pH 9.0, and 5 mM **30** for 2 h, cryoprotected with Paratone N, and flash cooled. Data were collected at beamline 21-ID-F of the Life Science Collaborative Access Team (LS-CAT) at the Advanced Photon Source (APS) using a 50 x 50 μm beam at wavelength

0.97856 Å and a MAR 300 CCD detector. A total of 360 frames were collected from 0 to 180° with an oscillation range of 0.5°. Data were integrated and scaled using HKL2000[5].

Initial phases for the SbAD^{Y252F} mutant were obtained by molecular replacement with SbAD WT (PDB ID 4ZBO) using Phaser[6, 7] of the CCP4 suite v7.0[8]. Iterative rounds of model building and refinement were performed in PHENIX[9, 10] and COOT[11, 12]. Geometry restraints for **30** bound covalently to the ε-amino group of K122 were generated with eLBOW[13]. Regions of the model for translation-liberation-screw (TLS) refinement were identified with phenix.find_tls_groups. The model was validated using tools implemented in COOT and MolProbity[14]. Data collection and refinement statistics are in Table **7**. Coordinates and structure factors are deposited in the Protein Data Bank as entry 6EEJ.

Results and Discussion

Substrate specificity of SbAD. Our preliminary investigation of SbAD's substrate preferences indicated that aromatic unsaturated aldehydes were the most efficient substrates (e.g. **4**, Scheme 1b). In this study we test additional aromatic aldehydes and investigate the influence of substituents on the aromatic ring, as well as those in the

aliphatic portions of the substrates. The results of steady state kinetics experiments with saturating pyruvate and the aldehydes shown in Scheme 2 are presented in Table 1. We had expected that the larger aromatic group of 2-benzofurancarboxaldehyde (**6**) relative to *trans*-3-(2-furyl)acrolein (**4**), together with the reduced number of rotatable bonds in the former, might result in improved binding to the enzyme. This proved not to be the case and, from the steady state data, it appears that **4** and **6** do not differ significantly. The next substrate, *trans*-cinnamaldehyde (**7**), gave a 23-fold decrease in K_M relative to **4**. Since the only difference between **4** and **7** is the aromatic moiety, the greater apparent affinity of SbAD for **7** is likely due to the larger aromatic group of **7** more fully occupying the funnel-like active site of SbAD. Differences in the solvation of **7** and **4** also likely contribute to the more favorable binding of **7**. Based on this result, **7** and its substituted analogs were used to investigate the impact of phenyl ring substituents on catalysis.

Scheme 2. Aldehyde substrates tested in steady state activity assays with SbAD.

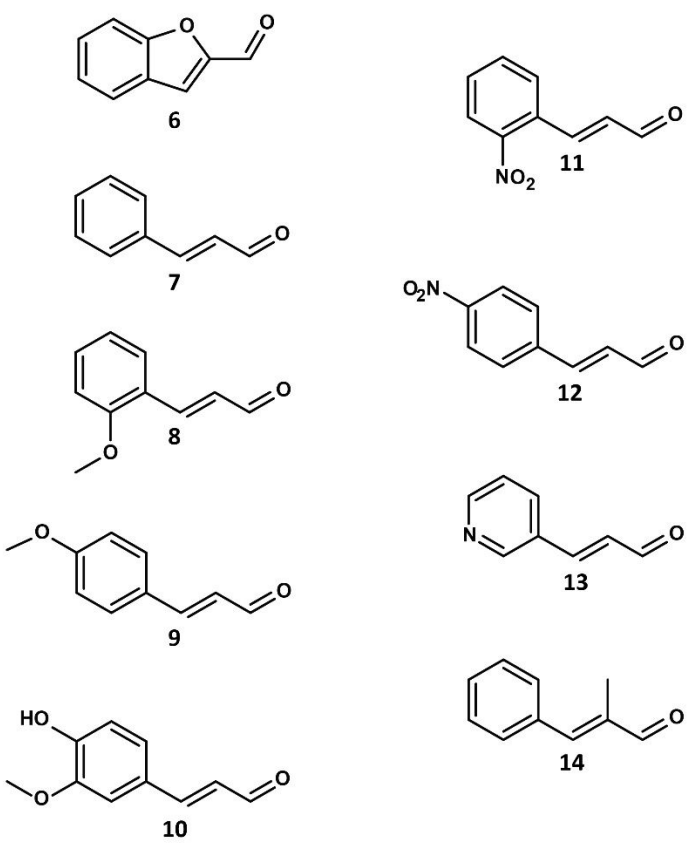

Overall, the substrates with *para* substituents had lower K_M values, while substituents in the *ortho* or *meta* positions increased K_M (Table 1). The *o*-methoxy substituent of 2-methoxycinnamaldehyde (**8**) and *p*-methoxy substituent of 4-methyoxycinnamaldehyde (**9**) appear to make these compounds more efficient substrates than the *meta* substitution of 3-methoxy-4-hydroxycinnamaldehyde (**10**), as judged by the higher pseudo-second-order rate constants for **8** and **9**. However, this assumes that the effect of the 4-hydroxyl group of **10** is negligible compared to the 3-methoxy interaction with the active site.

Consistent with this pattern, the *ortho*-nitro cinnamaldehyde (**11**) is a less efficient substrate than the *para*-nitro analog **12**. The K_M value for **12** is 10-fold lower, while the turnover number is roughly equivalent to that for **11**, resulting in an approximately 4-fold increase in k_{cat}/K_M for **12** (Table 1). Unfortunately, *meta*-nitro cinnamaldehyde was not commercially available for comparison with **11** and **12**.

Table 1. Steady state kinetic parameters measured for 0.1 μM SbAD in the presence of 50 mM pyruvate and various aldehyde substrates (Scheme 2). The steady state parameters for pyruvate were measured with saturating (1 mM) *trans*-cinnamaldehyde, **7**.

				Product	
Substrate	k_{cat} (s^{-1})	K_M (μM)	k_{cat}/K_M ($M^{-1}s^{-1}$)	λ_{mon} (nm)	ε ($M^{-1}cm^{-1}$)
4[a]	22.9 ± 0.8	1200 ± 80	1.9 ± 0.14 x 10^4	390	10062
6	7.3 ± 0.2	699.4 ± 45.7	1.0 ± 0.07 x 10^4	380	10749
7	28.3 ± 0.4	52.9 ± 1.6	5.4 ± 0.18 x 10^5	360	17050
8	15.7 ± 0.4	100.2 ± 4.0	1.6 ± 0.07 x 10^5	360	11908
9	3.3 ± 0.1	13.1 ± 0.9	2.5 ± 0.19 x 10^5	360	46035

10	1.7 ± 0.1	117.2 ± 19.6	1.5 ± 0.26 x 10^4	360	34851
11	24.7 ± 0.6	30.6 ± 3.0	8.1 ± 0.81 x 10^5	360	11963
12	10.2 ± 0.1	3.1 ± 0.1	3.3 ± 0.11 x 10^6	360	49616
13	221.9 ± 0.6	187.7 ± 1.8	1.2 ± 0.20 x 10^6	360	9077
14	2.0 ± 0.1	426.9 ± 58.8	4.7 ± 0.69 x 10^3	360	12624
3	22.3 ± 0.4	2914 ± 181	7.7 ± 0.49 x 10^3	360	-

[a] All reactions contained 0.1 μM SbAD in 100 mM bis-TRIS pH 6.5.

To test the effect of introducing an electronegative atom into the ring of **7**, we measured the steady state kinetics of SbAD with 3-(3-pyridyl)acrolein (**13**). While the K_M value does not differ significantly from that of **7** (Table 1), the k_{cat} value for **13** was approximately 400 s^{-1}, by far the highest of all the substrates tested. Though compound **13** is undoubtedly more electrophilic than **7** because of induction by the pyridine nitrogen, we suspect this is not the only factor. Compounds **11** and **12** bearing nitro substituents have k_{cat} values lower than unsubstituted **7**, and the electronically deactivated **8** and **9**, while having lower k_{cat} values than **7**, are not substantially lower in activity. The lower K_M values for the nitro derivatives **11** and **12** than for pyridyl **13** suggest that steric repulsion by these substituents is not a problem, at least in the ground state. It may be that pyridyl-

substituted **13** allows hydrogen bonding that stabilizes the transition state. That this does not lower K_M is consistent with competitive solvent hydrogen-bonding, or perhaps positioning for hydrogen-bonding only in a tetrahedral intermediate.

The structure of SbAD[1] shows that the active site funnel is quite narrow, and that any additions to the aliphatic portion of the cinnamaldehyde scaffold would be expected to have a negative impact on substrate binding and/or catalysis. To test this idea, we analyzed the steady state kinetics of SbAD with α-methyl-*trans*-cinnamaldehyde (**14**) and found that this compound is roughly two orders of magnitude worse than **7** in terms of k_{cat}/K_M. This results from the combined effects of an 8-fold increase in K_M and a 14-fold decrease in k_{cat}. The addition of the methyl group apparently not only interferes with binding of **14**, but also likely misorients the aldehyde function, hindering attack by the Schiff base enamine.

A number of compounds tested were found not to be substrates for SbAD (Scheme 3). Compounds **15-25** were tested at concentrations up to 2.5 mM with saturating (50 mM) pyruvate. Based on our previous results with benzaldehyde[1], it was expected that compounds **15-19** would be poor substrates, but the result with **13** led us to ask if the

same effect might operate on these small substrates. The observation that none of these compounds were substrates for SbAD supports the notion that the aliphatic portion of the cinnamaldehyde scaffold is required for activity. Compound **20** was tested as a comparison to 2-benzofurancarboxaldehyde (**6**), as well as to observe if nitrogen in the aromatic ring could increase k_{cat} as seen for **13** when compared to *trans*-cinnamaldehyde. Surprisingly, no activity was observed.

Scheme 3. Aldehydes tested for activity in the SbAD-catalyzed aldol condensation reaction and found not to be substrates.

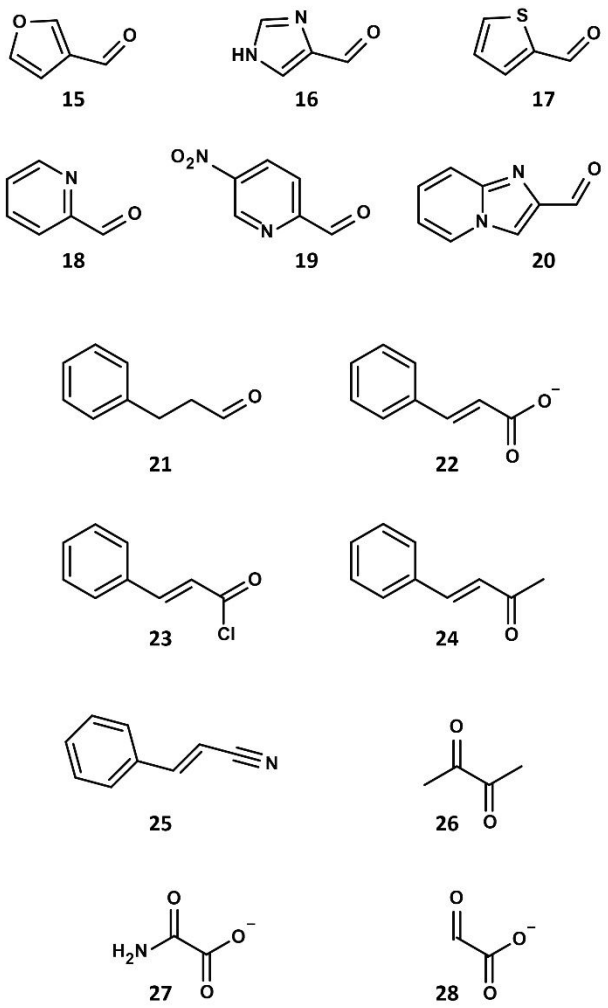

Compounds **21**-**25** were examined to test the hypothesis that SbAD could only catalyze the condensation of unsaturated, aliphatic aldehydes with pyruvate. Hydrocinnamaldehyde (**21**) was not a substrate for SbAD, although it is a substrate of the pyruvate-dependent *trans-o*-hydroxybenzylidenepyruvate hydratase-aldolase (tHBP-HA) of *Pseudomonas fluorescens* N3[15]. The condensation product of hydrocinnamaldehyde

and pyruvate with tHBP-HA, interestingly, has a furan derivative formed from the pyruvate moiety. This furan derivative cannot be formed by the tHBP-HA, and either forms spontaneously from the enol form of the condensation product, or by an intramolecular Michael reaction[15]. Although the structure of tHBP-HA has not been determined, sequence analysis and its similarity to N-acetylneuraminic acid aldolase[16, 17] suggest that tHBP-HA likely has an $(\alpha/\beta)_8$ barrel fold, like all known type I aldolases outside the ADCSF. The reason why SbAD does not react with **21** is likely due to the larger number of rotatable bonds in compound **21** compared to cinnamaldehyde (**7**). **21** may experience an entropic barrier to binding, or the increased flexibility may preclude productive binding of the aldehyde near the pyruvate enamine. SbAD is similar to tHBP-HA, however, in its specificity for pyruvate as the acceptor substrate[15]. There was no reaction of SbAD with saturating concentrations of *trans*-cinnamaldehyde (**7**) and 50 mM **26**-**28**. Glyoxylate (**28**) has been observed covalently bound to K122 in X-ray crystal structures (not shown), but as this is apparently an unproductive complex, it is not described here.

Kinetics of the retro-aldol cleavage reaction. As our first observation of SbAD activity was in the "reverse" or retro-aldol cleavage direction (Scheme 1a), we were interested to

more fully explore the kinetics of the reaction in this direction. The kinetics of SbAD-catalyzed retro-aldol cleavage of compounds **5**, **29** and **30** (Scheme 4) were measured in the steady state (Table 2). The retro-aldol cleavage of **30** was confirmed by reversed phase HPLC analysis (Figure 2). The pseudo-second order rate constants of **29** and **30** are an order of magnitude greater than that of **5**, perhaps due to enhanced van der Waals contacts with the phenyl rings of **29** and **30** relative to the furyl ring of **5**. The K_M values (Table 2) decrease 2-fold when the bulkiness of the aromatic group increases from **5** to **29**, and again when the nitro group is added (**30**), suggesting that the phenyl group of **29**, and particularly the *p*-nitro-phenyl group of **30**, more completely fill the binding pocket. It is also possible that the electron withdrawing group of **30** affects k_{cat} by drawing electron density out of the aldehyde group, increasing its electrophilicity. Comparing the steady state parameters in Table 2 with the values for the corresponding aldol condensation reactions (Table 1), it is evident that the turnover numbers for the retro-aldol cleavage of **29** and **30** are both 15-fold slower than the values for the condensation reactions. The K_M values for **29** and **7**, or **30** and **12** are more or less identical. Thus, it seems that the aldol condensation is kinetically favored to some extent over the retro-aldol cleavage. The K_{eq}

values obtained experimentally, and from the Haldane relationship[18] in the reversible aldol condensation of pyruvate and **12** to produce **30**, indicate that the aldolase-dehydratase reaction is favored when pyruvate is in excess. Given the observation that pyruvate concentrations in living cells can be in the low millimolar range[19, 20], it is likely that the aldol condensation is the physiologically relevant reaction of SbAD. The K_{eq} lying toward condensation when pyruvate is in excess is consistent with other Class I (lysine-dependent) pyruvate aldolases like N-acetylneuraminic acid aldolase[17, 21] and *trans-o*-hydroxybenzylidenepyruvate hydratase-aldolase[17, 22].

Scheme 4. Dieneone compounds tested for activity in the SbAD-catalyzed retro-aldol cleavage reaction.

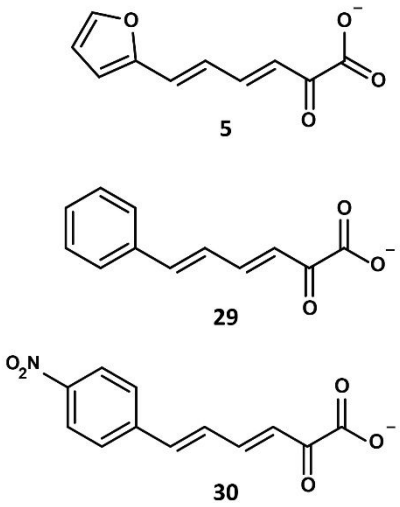

Table 2. Steady state kinetic parameters measured for the dehydration of 0.1 μM SbAD with **5**, **29**, and **30**.

				Product	
Substrate	k_{cat} (s^{-1})	K_M (μM)	k_{cat}/K_M ($M^{-1}s^{-1}$)	λ_{mon} (nm)	ε ($M^{-1}cm^{-1}$)
5	0.21 ± 0.02	52.9 ± 8.3	4.0×10^3	390	10062
29	1.57 ± 0.04	24.9 ± 1.7	6.3×10^4	360	17050
30	0.68 ± 0.04	8.5 ± 0.9	8.0×10^4	360	49616

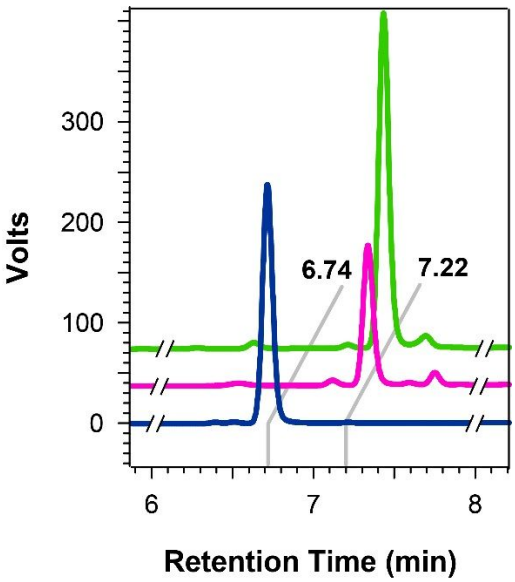

Figure 2. Reversed phase HPLC chromatograms showing SbAD-catalyzed aldol condensation of pyruvate and **12**. The authentic **12** standard (blue trace) elutes at 6.74 min, while authentic **30** elutes at 7.22 min (magenta trace). Standards were 200 μM in 100 mM MOPS pH 7.0. A reaction containing 10 μM SbAD, 100 mM pyruvate, and 200 μM **12**, was prepared in 100 mM MOPS pH 7.0 (green trace). After standing at RT for 20h, only the condensation product **30** is detectable.

Site-directed mutagenesis studies. Site-directed mutagenesis was used to explore the roles of specific active site residues in catalysis. Y82 was examined for its potential hydrogen bonding contribution to the carboxylate binding site, as observed in the

structure of wild-type SbAD with pyruvate covalently bound to the active site lysine (PDB ID 4ZBT [1]). The steady state kinetics of the SbAD^{Y82F} variant in the aldol condensation of **12** with saturating pyruvate (Table 3) and the retro-aldol cleavage of **30** (Table 4) do not vary significantly from WT. Therefore, Y82 is either not important for activity or there are compensating interactions such that the loss of Y82 has no impact on the steady state kinetics. Examination of other active site variants of SbAD was done in the context of the condensation of **7** with pyruvate, and the cleavage of **29**, due to better solubility of **29** and ability to perform assays at room temperature rather than 4°C. Tables 3 and 4 list the steady state parameters for wild-type SbAD and the single- and double-mutant variants examined here. Binding constants for pyruvate and **7** were measured for all variants by intrinsic fluorescence titration (Table 5).

Table 3. Steady state kinetics for wild-type and mutant SbAD in the aldolase-dehydratase reaction with 50 mM pyruvate (**3**) and either **12** or **7**.

SbAD	Substrate	k_{cat} (s^{-1})	K_M (μM)	k_{cat}/K_M ($M^{-1}s^{-1}$)
WT	**12**[a]	6.3 ± 0.1	2.9 ± 0.7	2.2 x 10^6

Y82F	**12**[a]	13.9 ± 0.3	11.8 ± 1.0	1.2×10^6
WT	**7**	23.0 ± 0.4	38.4 ± 2.0	6.0×10^5
E84Q	**7**	2.52 ± 0.02	38.9 ± 1.1	6.5×10^4
Q118N	**7**	0.214 ± 0.006	52.9 ± 5.2	4.1×10^3
Y252F	**7**	1.45 ± 0.01	5.4 ± 0.7	2.7×10^5
Y82F/Y252F	**7**	1.20 ± 0.02	7.2 ± 0.8	1.7×10^5
E84Q/Y252F	**7**	No Activity		

[a]Reactions were performed at 4°C; all others were performed at 20°C.

Table 4. Steady state kinetics for SbAD WT and mutants in the hydratase-retroaldolase reaction.

SbAD	Substrate	k_{cat} (s^{-1})	K_M (μM)	k_{cat}/K_M ($M^{-1}s^{-1}$)
WT	**30**[a]	1.9 ± 0.5	82.3 ± 29.1	2.3×10^4
Y82F	**30**[a]	1.9 ± 0.2	75.1 ± 9.2	2.5×10^4
WT	**29**	1.1 ± 0.1	15.4 ± 2.0	7.4×10^4
E84Q	**29**	0.56 ± 0.02	27.1 ± 1.9	2.1×10^4
Q118N	**29**	0.37 ± 0.03	16.6 ± 3.3	2.2×10^4
Y252F	**29**	0.74 ± 0.02	4.8 ± 0.4	1.5×10^5
Y82F/Y252F	**29**	0.53 ± 0.04	26.4 ± 4.6	2.0×10^4
E84Q/Y252F	**29**	No Activity		

[a] Reactions were performed at 4°C; all others were performed at 20°C.

Table 5. K_D values for SbAD WT and mutants.

SbAD	3 (mM)	*7* (μM)
WT	6.5 ± 0.6	58.2 ± 6.7
Y82F	1.9 ± 0.3	81.8 ± 8.7

E84Q	5.3 ± 1.1	56.6 ± 3.2
Q118N	5.4 ± 1.0	73.9 ± 6.7
K122M[a]	11.3 ± 1.8	87.3 ± 9.6
Y252F	5.5 ± 0.9	41.7 ± 3.0
E84Q/Y252F	54.7 ± 6.0	93.2 ± 9.3

[a]K122M had no activity in either condensation or retro-aldol reactions and was generated specifically for binding studies.

Formation of the Schiff base should require the aid of a general base catalyst, and the most likely candidate for this role in SbAD is E84. We expected a significant decrease in k_{cat} if E84 were the only residue available to participate in the Schiff-base chemistry. However, the steady state kinetics of $SbAD^{E84Q}$ were very similar to the wild-type, with only a 10-fold decrease in k_{cat} for the condensation reaction and no significant effect on K_M. Interestingly, the retro-aldol cleavage reaction for $SbAD^{E84Q}$ doubled the K_M for cinnamylidenepyruvate (**29**) and halved the turnover number (Table 4). The binding constants of $SbAD^{E84Q}$ are also almost identical to the wild-type (Table 5), indicating that

E84 is not required for substrate binding. The stability of wild-type SbAD and SbAD^{E84Q} were assessed by differential scanning calorimetry in the absence of substrate (Supplemental Materials and Methods). The melting temperature (T_M) for wild-type SbAD was 53.4 ± 0.6 °C. The T_M of SbAD^{E84Q} was 45.4 ± 0.1 °C (Table S2). The decrease in melting temperature for SbAD^{E84Q} indicates that the mutant enzyme is somewhat less stable than the wild-type, however all kinetics experiments were performed at 20 °C, well below the temperature where the mutant would be expected to undergo significant denaturation. It should also be noted that the E84Q mutant gave diffraction-quality crystals at 22°C (data not shown), further suggesting that effects observed in the kinetics of the E84Q mutant are not due to thermal denaturation.

Q118 makes a hydrogen bonding interaction to the pyruvate carboxylate group as part of the carboxylate-binding site, as well as the carbonyl of R114 (PDB ID 4ZBT). The guanidinium group of R114 forms a salt bridge to the pyruvate carboxylate. Another acetoacetate decarboxylase-like superfamily enzyme, Swit_4259, naturally has Asn at position 118 (same numbering in both Swit_4259 and SbAD) and has aldolase-dehydratase function like SbAD[3]. Swit_4259, however, has a more disordered active site

(PDB ID 5UPB) and it was not possible to trap Schiff base complexes crystallographically. Thus, the Q118N mutation was made to see if the SbAD carboxylate-binding site would become disordered like that of Swit_4259. If so, we predicted that SbAD^{Q118N} would have decreased activity. Experimental results validated this hypothesis, as SbAD^{Q118N} had dramatically lower k_{cat} values in both the condensation and retro-aldol cleavage reactions (Tables 3 and 4), with similar K_D values for pyruvate and *trans*-cinnamaldehyde (Table 5). The latter observation was somewhat surprising, since it was expected that breaking the pre-ordered pyruvate-binding site would impact the binding constant, but it did not. Together, these observations imply that Q118 is a catalytically significant residue, either directly or by positioning the carboxylate to participate in the reaction as observed in sialic acid aldolase[23] and proposed earlier for SbAD[1].

As anticipated, the K122M mutation abolished activity, since this variant has no reactive amine to perform the Schiff base chemistry. The K_D values of SbAD WT and SbAD^{K122M} for pyruvate and *trans*-cinnamaldehyde are similar (Table 5), which is surprising given that SbAD^{K122M} cannot bind pyruvate covalently. This suggests that the carboxylate-

binding site of SbAD, residues Y24, Y82, R114, and Q118, are largely responsible for pyruvate binding and not the covalent bond formed to K122.

The residue at position 252 (Y252 in SbAD) has been proposed as a "specificity-determining" residue in the Family V ADCSF enzymes [1, 3]. Y252 of SbAD was observed to interact with a conserved water molecule in the formate- and pyruvate-bound structures of SbAD (PDB ID 4ZBO and 4ZBT, respectively[1]). These structures prompted us to propose that Y252 may be involved in binding the incoming aldehyde and/or positioning it for attack by the pyruvate enamine. The SbAD^{Y252F} variant was examined in order to test this hypothesis. The data in tables 3 and 4 indicate that the Y252F change had only a mild effect on turnover. The effect on k_{cat} was about 10-fold greater for the condensation reaction than the retro-aldol cleavage, suggesting that the phenolic oxygen of Y252 likely does play a role in optimizing the orientation of the aldehyde group for catalysis, though this role is not essential.

The mild effects observed with the E84Q and Y252F variants for SbAD led us to combine these mutations in order to see if the effects were additive or synergistic. When the SbAD$^{E84Q/Y252F}$ variant was tested in the steady state kinetics assays, there was no

detectable enzymatic activity (Tables 3 and 4). Interestingly, the K_D value for pyruvate binding to the E84Q/Y252F variant increased by almost an order of magnitude. This was surprising, because neither the E84Q nor the Y252F variant showed any change in the dissociation constant for pyruvate and the dissociation constant for cinnamaldehyde (**7**) was unaffected. Perhaps Y252 is important not only for orienting the incoming aldehyde, but also for facilitating access of pyruvate to the catalytic lysine in what is an otherwise very hydrophobic active site.

Pre-steady state kinetics. Identification of **12** as a very efficient substrate prompted us to study the pre-steady state kinetics of SbAD. Single turnover transient kinetics were measured to determine if any intermediates could be detected in the reaction. Mixing excess SbAD (100 μM, all concentrations after mixing) with limiting **30** resulted in a decrease in absorbance at 350 nm, the λ_{max} of **30**, and concomitant increase in absorbance at 415 nm (Figure 3A). We propose that that species with λ_{max} at 415 nm is the Schiff base between the enzyme and what would become the dienone product upon hydrolysis. Since the species absorbing at 415 nm was observed to accumulate, we reasoned that if it were truly an enzyme-bound intermediate, then we should observe

burst kinetics. When varying concentrations of enzyme (1.25 – 5.0 μM) were mixed with saturating amounts of **7** (500 μM) and pyruvate (200 mM), a kinetic burst was observed at 430 nm (Figure 3B). Observations were made at 430 nm to minimize background absorbance from **30**. The data in Figure 3B and Table 6 indicate that the reaction is enzyme catalyzed, as the amplitude and steady state rate double as the enzyme concentration doubles. The extinction coefficient of the intermediate is not known, so it is impossible to determine if the Y-intercepts of the steady state portions of the traces correspond to their respective enzyme concentrations. Burst kinetics indicate a covalent intermediate in the reaction or that product release is rate-limiting.

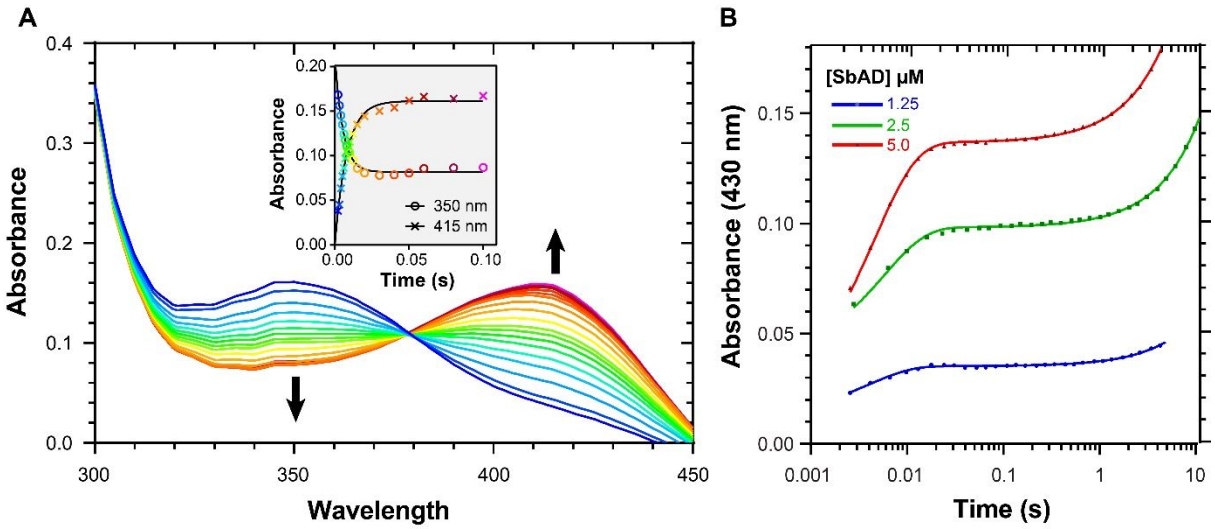

Figure 3. Pre-steady state kinetics of SbAD-catalyzed retro-aldol cleavage of **30**. When wild-type SbAD was mixed with **30** (100 μM and 20 μM, respectively, after mixing) the absorbance at 350 nm, due to **30**, decreased and the absorbance at 415 nm increased (A). The data begin at 2 ms (blue) and end at 100 ms (magenta). The inset shows the time course of these spectral changes. Burst kinetics were observed when limiting amounts of wild-type SbAD (1.25 μM [blue], 2.5 μM [green], or 5.0 μM [red]) were mixed with saturating amounts of pyruvate (200 mM) and cinnamaldehyde (2.5 mM) (B). Only every 20th data point is plotted to better show the non-linear fits. All reactions were performed in 100 mM Bis-TRIS pH 6.5.

Table 6. Burst kinetics were observed with saturating pyruvate (200mM) and **7** (500 μM).

$$y = -A\,e^{(-kt)} + mx + C$$

[SbAD WT] (μM)	1.25	2.5	5.0
Amplitude (A)	0.022 ± 0.003	0.059 ± 0.001	0.117 ± 0.006
Burst rate (k, s^{-1})	242 ± 4	191 ± 2	213 ± 1
Steady state rate (m, Abs s^{-1})	0.002 ± 1.0 x 10^{-5}	0.005 ± 1.0 x 10^{-5}	0.010 ± 2 x 10^{-5}

*Structure of Schiff base intermediate with **30**.* The observation that the intermediate at 415 nm persisted for relatively long periods of time, especially in the $SbAD^{Y252F}$ variant, led us to attempt trapping this species crystallographically (Figure 4). $SbAD^{Y252F}$ was crystallized in the same manner as WT[1], and soaked in 5 mM **30** for two h before flash cooling. Data processing and model refinement statistics are given in Table 7. The crystal structure of $SbAD^{Y252F}$ was obtained with **30** covalently bound to the active site K122 in all 4 molecules in the asymmetric unit. The condensation product trapped in the active site of chain B is pictured in Figures 3 and 4, where the red loop (residues 169-180) marks the surface of the protein and mouth of the active site. The Y252F mutation is clearly

visible in the electron density (red label in Figures 3 and 4). Aside from the carboxylate-binding site, the rest of the active site is hydrophobic and binding of the condensation product is predominantly by van der Waals interactions (Figure 5). It may be that this complex is trapped because the phenolic hydroxyl group of Y252 is not there to promote hydration of the double bond by keeping a water molecule at the correct position in an otherwise hydrophobic active site. Thus, Y252 appears to have a catalytic role. The torsion angles of the bound product are intriguing (Figure 6 and Table 8). Given that the crystal used to collect the diffraction data was bright yellow, we had expected **30** to be bound in a planar conformation consistent with the high degree of conjugation. However, the torsion angle labeled as '4' in Figure 6 is near 90 °. This suggests that SbAD may destabilize **30** by breaking up the conjugation of the ring system prior to hydration of the double bond and retro-aldol cleavage.

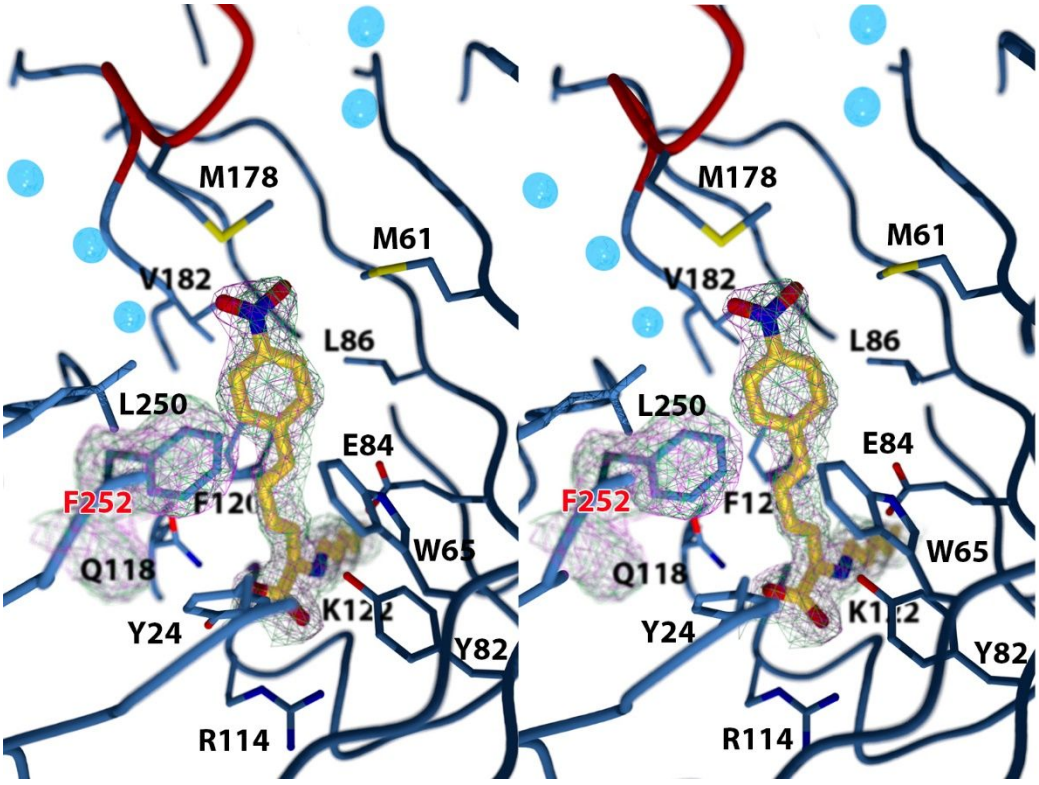

Figure 4. Crystal structure of SbAD^{Y252F} with the **30**-derived intermediate bound in the active site. $2F_o$-F_c electron density is in magenta and simulated annealing omit electron density is in green. Both are contoured at 1.2σ. Selected water molecules (blue spheres) are shown to highlight the paths to the bulk solvent on either side of the active site loop (red).

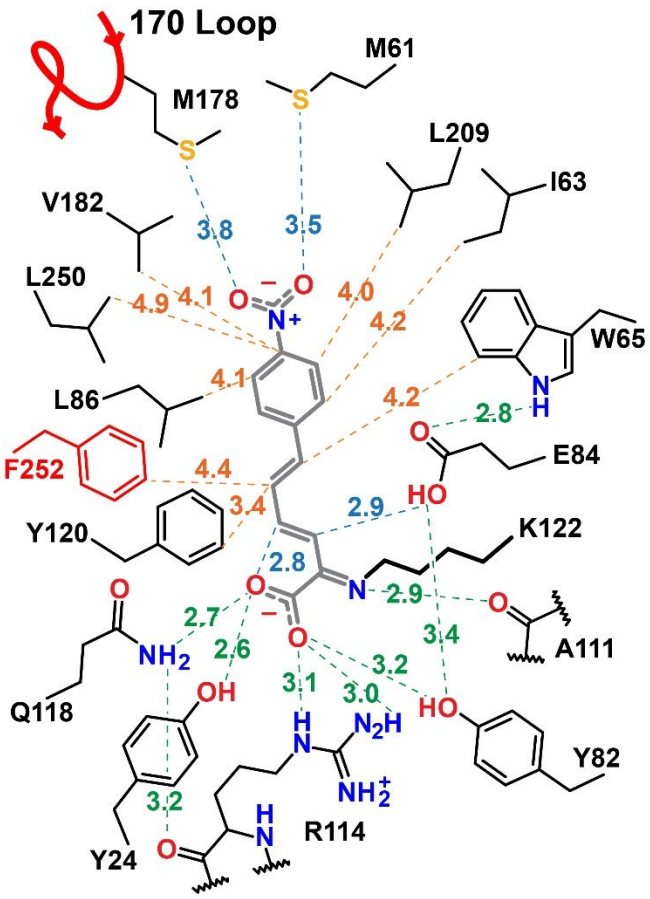

Figure 5. Interactions between the **30**-derived intermediate and the SbAD^{Y252F} active site. Hydrogen bonding interactions are shown as green, dotted lines with associated donor-acceptor distances in Å. Orange, dotted lines represent hydrophobic contacts, and blue, dotted lines are informational and do not represent any type of interaction.

Table 7. Crystallographic data collection and model refinement statistics for SbAD Y252F covalently complexed with **30**.

Data collection	
Resolution range (Å) (last shell)[a]	48.79 – 1.89 (1.96 – 1.892)
Space Group	P 2_1 2_1 2
a, *b*, *c* (Å)	157.1, 123.7, 53.1
α, β, γ (°)	90, 90, 90
R_{merge}[a,b]	0.129 (0.553)
R_{meas}	0.139 (0.599)
R_{pim}	0.052 (0.228)
$CC_{1/2}$	0.994 (0.84)
Total No. of reflections	595865 (54470)
No. of unique reflections	83236 (7582)
Completeness (%)[a]	99.15 (92.31)
Multiplicity	7.2 (6.8)
$\langle I/\sigma(I) \rangle$[a]	17.3 (3.5)
Model Refinement	
Reflections used in refinement	82767 (7582)
Reflections used for R_{free}	2000 (183)

R_{cryst} (R_{free})	0.162 (0.181)
Wilson B-factor (Å^2)	17.7
Number of TLS groups	24
Average B factor (Å^2)[c]	20.75
Protein atoms	19.04
Solvent	31.40
Ligand	28.63
Root-mean-square (RMSD) deviations	
Bond lengths (Å)	0.002
Bond angles (°)	0.615
Coordinate error (Å)	0.14
Ramachandran statistics	
Favored/allowed/outliers (%)	97.2/2.8/0.0
Rotamer outliers (%)	1.11
Clashscore	1.40

[a]Values in parentheses apply to the high-resolution shell indicated in the resolution row

[b]$R = \sum(||F_{obs}| - \text{scale} \times |F_{calc}||)/\sum|F_{obs}|$.

[c]Isotropic equivalent B factors, including the contribution from TLS refinement

Table 8. Values of the dihedral were averaged over the four active sites in the crystallographic asymmetric unit. The torsion angles are labeled in Figure 6.

Torsion angles	Average (°)	Range (°)
1	169.9 ± 3.0	166.4 – 173.3
2	163.7 ± 5.1	156.2 – 167.8
3	164.8 ± 2.8	161.6 – 167.9
4	82.4 ± 12.8	72.2 – 100.5
5	175.2 ± 2.5	171.5 – 176.8
6	34.4 ± 13.1	19.1 – 48.0

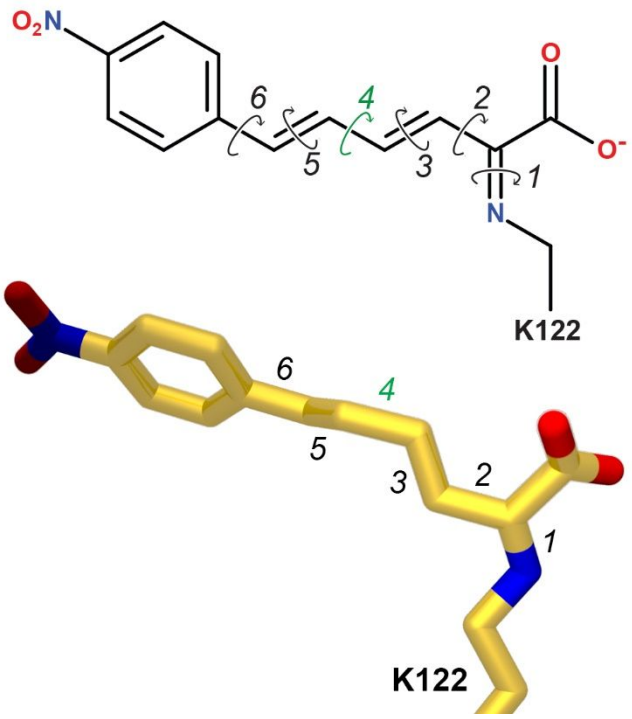

Figure 6. The proposed intermediate based on the crystal structure. The dihedral angles corresponding to numbers *1-6* are listed in Table 8.

Proposed mechanism of SbAD. Based on the steady state and pre-steady state kinetics, and the structure of the intermediate covalently bound to $SbAD^{Y252F}$, we propose that SbAD uses a mechanism similar to other Class I pyruvate-dependent aldolases. The proposed reaction mechanism with relevant active site residues is depicted in Figure 7. The order of addition of pyruvate and the aldehyde have yet to be determined, but the

narrowness of the active site suggests that pyruvate likely binds before the aldehyde. Pyruvate binding rapidly triggers Schiff base formation, after which the nucleophilic enamine attacks the carbonyl of the incoming aldehyde. The condensation results in a primary alcohol that is eliminated as water. Water near the catalytic K122 then hydrolyzes the Schiff base to release the dienone product and regenerate the enzyme. Catalytic roles for E84 and Y252 have been assigned based on the mutagenesis experiments described above, where the E84Q/Y252F double mutant was completely inactive.

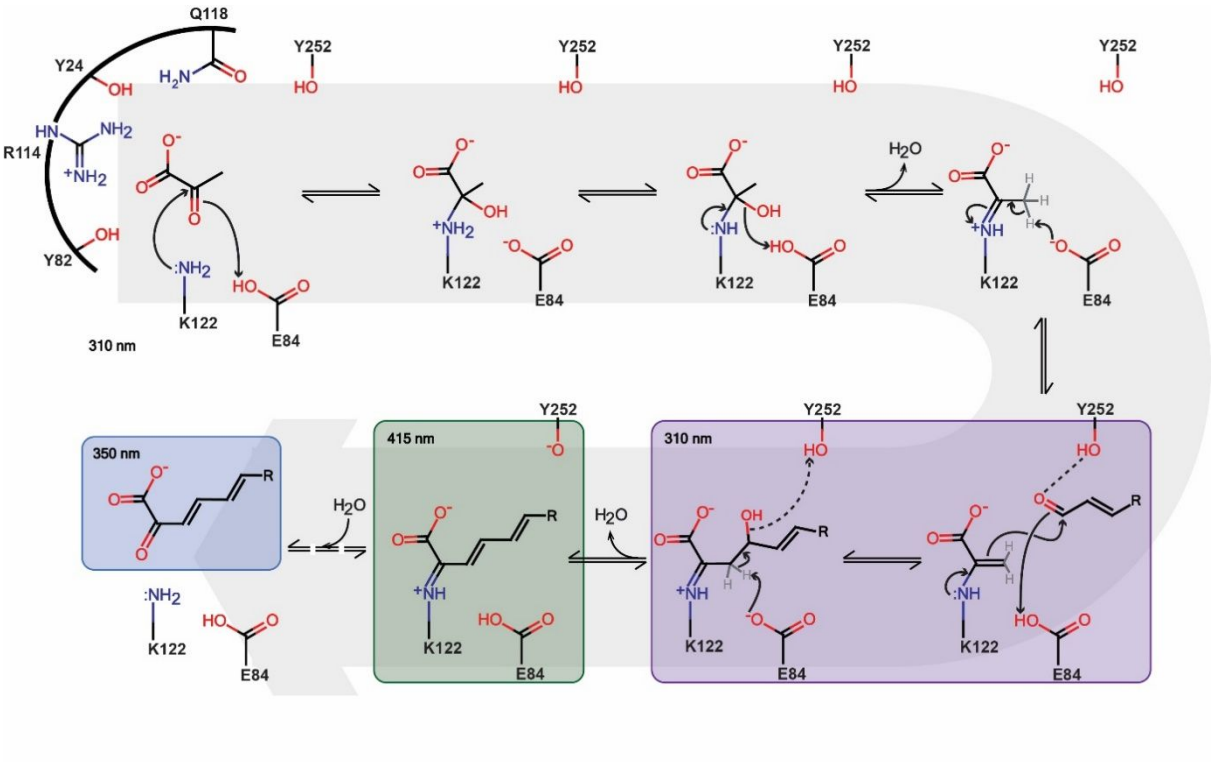

Figure 7. The proposed mechanism of SbAD. R represents phenyl (*i.e.* **29**) or *p*-nitrophenyl (*i.e.* **30**).

Conclusions

SbAD retains the Schiff-base chemistry observed in the prototypical acetoacetate decarboxylases due to its K122-E84 catalytic dyad, the only two active site residues shared between the classical and MppR-like ADCSF enzymes. However, the remaining architecture of the SbAD active site leads to differentiation in both substrate specificity and chemistry. The most efficient substrates to react with pyruvate were aromatic, unsaturated aliphatic aldehydes like *trans*-cinnamaldehyde with electron withdrawing groups in the *ortho* or *para* position of the phenyl ring. Site-specific mutations of residues in the carboxylate-binding site elaborated upon the proposed mechanism of SbAD. Y82 contributes to the carboxylate binding site, however its hydrogen bonding potential is not crucial to binding or catalysis. E84 is important for the Schiff base chemistry, however its mutation did not abolish function, so other nearby residues may be able to fill this role.

Y252 likely aids in orienting the incoming aldehyde for nucleophilc attack and likely helps recruit water to hydrate the double bond in the retro-aldol cleavage reaction. The crystal structure of SbAD with the conjugated intermediate supports this conclusion.

AUTHOR INFORMATION

Corresponding Author

To whom correspondence should be addressed: Nicholas R. Silvaggi, Ph.D.: 3210 North Cramer Street, Milwaukee, WI 53211, 414-229-2647, silvaggi@uwm.edu.

Present Addresses

†If an author's address is different than the one given in the affiliation line, this information may be included here.

Author Contributions

NRS designed the project. LSM performed biochemical assays and protein crystallization. LSM and NRS analyzed the data and solved the structure. AWS conceived of and supervised the organic synthesis. RWH and TMH synthesized and purified **29** and **30**. LSM, NRS, TMH, and AWS wrote the manuscript.

Funding Sources

This work was supported by grant MCB-1157392 from the National Science Foundation, Directorate of Biological Sciences.

ACKNOWLEDGMENT

We are grateful to Dr. Graham R. Moran for use of his stopped flow instrument to perform kinetics and fluorimeter to obtain binding constants. We also appreciate the use of the DSC from Dr. David Frick and use from Dr. William Sheldrick. Use of the Advanced Photon Source, an Office of Science User Facility operated for the U.S. Department of Energy (DOE) Office of Science by Argonne National Laboratory, was supported by the U.S. DOE under Contract No. DE-AC02-06CH11357. Use of the LS-CAT Sector 21 was supported by the Michigan Economic Development Corporation and the Michigan Technology Tri-Corridor (Grant 085P1000817).

ACCESSION CODES

SbAD D7C0E5

ABBREVIATIONS

ADCSF, acetoacetate decarboxylase-like superfamily; ShMppR, *Streptomyces hygroscopicus* MppR; t-HBP-HA, *trans-o*-hydroxybenzylidenepyruvate hydratase-aldolase

REFERENCES

[1] Mueller, L. S., Hoppe, R. W., Ochsenwald, J. M., Berndt, R. T., Severin, G. B., Schwabacher, A. W., and Silvaggi, N. R. (2015) Sbi00515, a Protein of Unknown Function from Streptomyces bingchenggensis, Highlights the Functional Versatility of the Acetoacetate Decarboxylase Scaffold, *Biochemistry 54*, 3978-3988.

[2] Burroughs, A. M., Hoppe, R. W., Goebel, N. C., Sayyed, B. H., Voegtline, T. J., Schwabacher, A. W., Zabriskie, T. M., and Silvaggi, N. R. (2013) Structural and functional characterization of MppR, an enduracididine biosynthetic enzyme from streptomyces hygroscopicus: functional diversity in the acetoacetate decarboxylase-like superfamily, *Biochemistry 52*, 4492-4506.

[3] Mydy, L. S., Mashhadi, Z., Knight, T. W., Fenske, T., Hagemann, T., Hoppe, R. W., Han, L., Miller, T. R., Schwabacher, A. W., and Silvaggi, N. R. (2017) Swit_4259, an acetoacetate decarboxylase-like enzyme from Sphingomonas wittichii RW1, *Acta crystallographica. Section F, Structural biology communications 73*, 672-681.

[4] Ho, M. C., Menetret, J. F., Tsuruta, H., and Allen, K. N. (2009) The origin of the electrostatic perturbation in acetoacetate decarboxylase, *Nature 459*, 393-397.

[5] Otwinowski, Z. M., W. (1997) Processing of X-ray diffraction data collected in oscillation mode, *Methods in enzymology 276*, 307–326.

[6] McCoy, A. J., Grosse-Kunstleve, R. W., Adams, P. D., Winn, M. D., Storoni, L. C., and Read, R. J. (2007) Phaser crystallographic software, *J Appl Crystallogr 40*, 658-674.

[7] McCoy, A. J. (2017) Acknowledging Errors: Advanced Molecular Replacement with Phaser, *Methods Mol Biol 1607*, 421-453.

[8] Winn, M. D., Ballard, C. C., Cowtan, K. D., Dodson, E. J., Emsley, P., Evans, P. R., Keegan, R. M., Krissinel, E. B., Leslie, A. G., McCoy, A., McNicholas, S. J., Murshudov, G. N., Pannu, N. S., Potterton, E. A., Powell, H. R., Read, R. J., Vagin, A., and Wilson, K. S. (2011) Overview of the CCP4 suite and current developments, *Acta Crystallogr D Biol Crystallogr 67*, 235-242.

[9] Adams, P. D., Afonine, P. V., Bunkoczi, G., Chen, V. B., Davis, I. W., Echols, N., Headd, J. J., Hung, L. W., Kapral, G. J., Grosse-Kunstleve, R. W., McCoy, A. J., Moriarty, N. W., Oeffner, R., Read, R. J., Richardson, D. C., Richardson, J. S., Terwilliger, T. C., and Zwart, P. H. (2010) PHENIX: a comprehensive Python-based system for macromolecular structure solution, *Acta Crystallogr D Biol Crystallogr 66*, 213-221.

[10] Afonine, P. V., Mustyakimov, M., Grosse-Kunstleve, R. W., Moriarty, N. W., Langan, P., and Adams, P. D. (2010) Joint X-ray and neutron refinement with phenix.refine, *Acta Crystallogr D Biol Crystallogr 66*, 1153-1163.

[11] Emsley, P., and Cowtan, K. (2004) Coot: model-building tools for molecular graphics, *Acta Crystallogr D Biol Crystallogr 60*, 2126-2132.

[12] Emsley, P., Lohkamp, B., Scott, W. G., and Cowtan, K. (2010) Features and development of Coot, *Acta Crystallogr D Biol Crystallogr 66*, 486-501.

[13] Moriarty, N. W., Grosse-Kunstleve, R. W., and Adams, P. D. (2009) electronic Ligand Builder and Optimization Workbench (eLBOW): a tool for ligand coordinate and restraint generation, *Acta Crystallogr D Biol Crystallogr 65*, 1074-1080.

[14] Chen, V. B., Arendall, W. B., 3rd, Headd, J. J., Keedy, D. A., Immormino, R. M., Kapral, G. J., Murray, L. W., Richardson, J. S., and Richardson, D. C. (2010) MolProbity: all-atom structure validation for macromolecular crystallography, *Acta Crystallogr D Biol Crystallogr 66*, 12-21.

[15] Sello, G., and Di Gennaro, P. (2013) Aldol reactions of the trans-o-hydroxybenzylidenepyruvate hydratase-aldolase (tHBP-HA) from Pseudomonas fluorescens N3, *Appl. Biochem. Biotechnol. 170*, 1702-1712.

[16] Ferrara, S., Mapelli, E., Sello, G., and Di Gennaro, P. (2011) Characterization of the aldol condensation activity of the trans-o-hydroxybenzylidenepyruvate hydratase-aldolase (tHBP-HA) cloned from Pseudomonas fluorescens N3, *Biochim Biophys Acta 1814*, 622-629.

[17] Lawrence, M. C., Barbosa, J. A., Smith, B. J., Hall, N. E., Pilling, P. A., Ooi, H. C., and Marcuccio, S. M. (1997) Structure and mechanism of a sub-family of enzymes related to N-acetylneuraminate lyase, *J Mol Biol 266*, 381-399.

[18] Cornish-Bowden, A. (2012) *Fundamentals of Enzyme Kinetics*, Fourth ed., Wiley-Blackwell, Weinheim, Germany.

[19] Roy, S. O., and Packard, T. T. (1998) NADP-Isocitrate dehydrogenase from Pseudomonas nautica: kinetic constant determination and carbon limitation effects on the pool of intracellular substrates, *Applied and environmental microbiology 64*, 4958-4964.

[20] Yasid, N. A., Rolfe, M. D., Green, J., and Williamson, M. P. (2016) Homeostasis of metabolites in Escherichia coli on transition from anaerobic to aerobic conditions and the transient secretion of pyruvate, *R Soc Open Sci 3*, 160187.

[21] Ji, W., Sun, W., Feng, J., Song, T., Zhang, D., Ouyang, P., Gu, Z., and Xie, J. (2015) Characterization of a novel N-acetylneuraminic acid lyase favoring industrial N-acetylneuraminic acid synthesis, *Sci Rep 5*, 9341.

[22] Eaton, R. W. (2000) trans-o-Hydroxybenzylidenepyruvate hydratase-aldolase as a biocatalyst, *Appl. Environ. Microbiol. 66*, 2668-2672.

[23] Smith, B. J., Lawrence, M. C., and Barbosa, J. A. (1999) Substrate-Assisted Catalysis in Sialic Acid Aldolase, *J. Org. Chem. 64*, 945-949.

Table of Contents Use Only

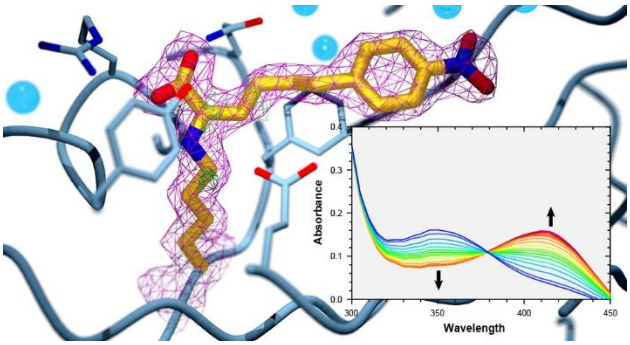
Absorbance
Wavelength
0.0
0.1
0.2
0.3
0.4
300
350
400
450

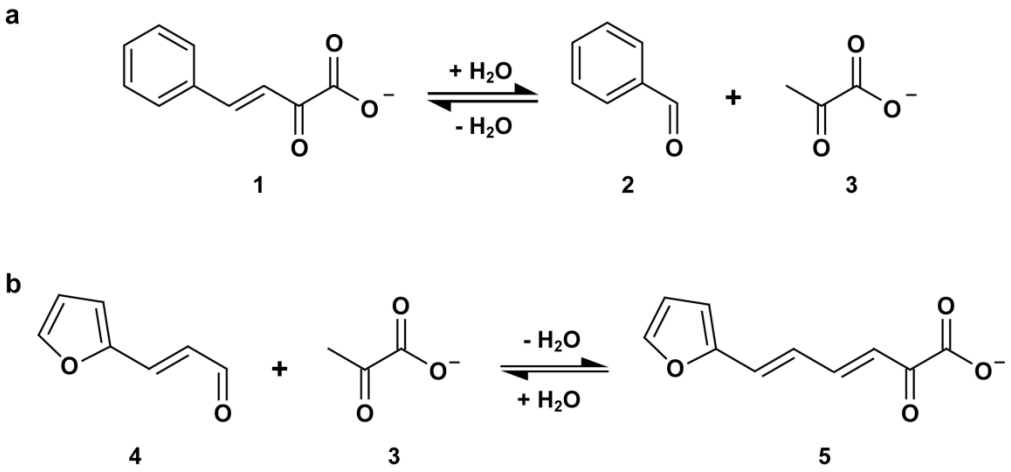

Scheme 1. Reactions catalyzed by SbAD.

181x85mm (300 x 300 DPI)

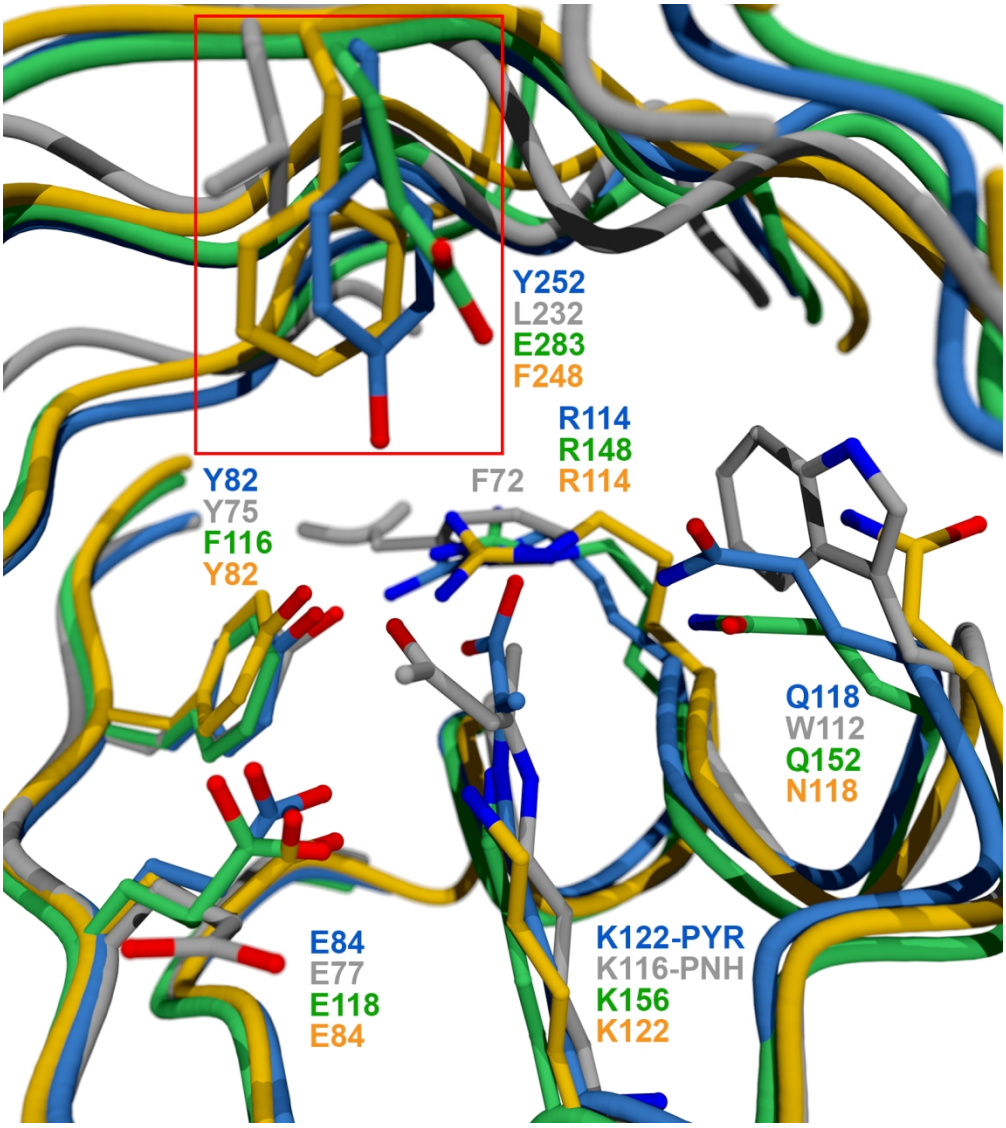

Figure 1. The active sites of four ADCSF enzymes are overlayed in order to highlight the similarities and differences in their active site architectures. The Schiff base complex between SbAD K122 and pyruvate is shown in blue (PDB ID 4ZBT). The analogous complex between the confirmed acetoacetate decarboxylase CvADC K116 and the substrate analog acetylacetate is shown in grey (PDB ID 3BH3). The unliganded structures of MppR (PDB ID 4JM3) and Swit_4259 (PDB ID 5UPB) are shown in green and yellow, respectively. Notice that the acetyl group of acetylacetone, which takes the place of the carboxylate of acetoacetate, points in the opposite direction from the carboxylate group of pyruvate. This is primarily due to the carboxylate-binding site formed by R114 and Q118 (SbAD numbering) in the MppR-like ADCSF enzymes. This subsite of the active site distinguishes the MppR-like enzymes from the bona fide acetoacetate decarboxylases. The position occupied by Y252 in SbAD (red box) constitutes one of the main differences between the active sites of enzymes within the MppR-like family of the ADCSF, such as SbAD, MppR, and Swit_4259.

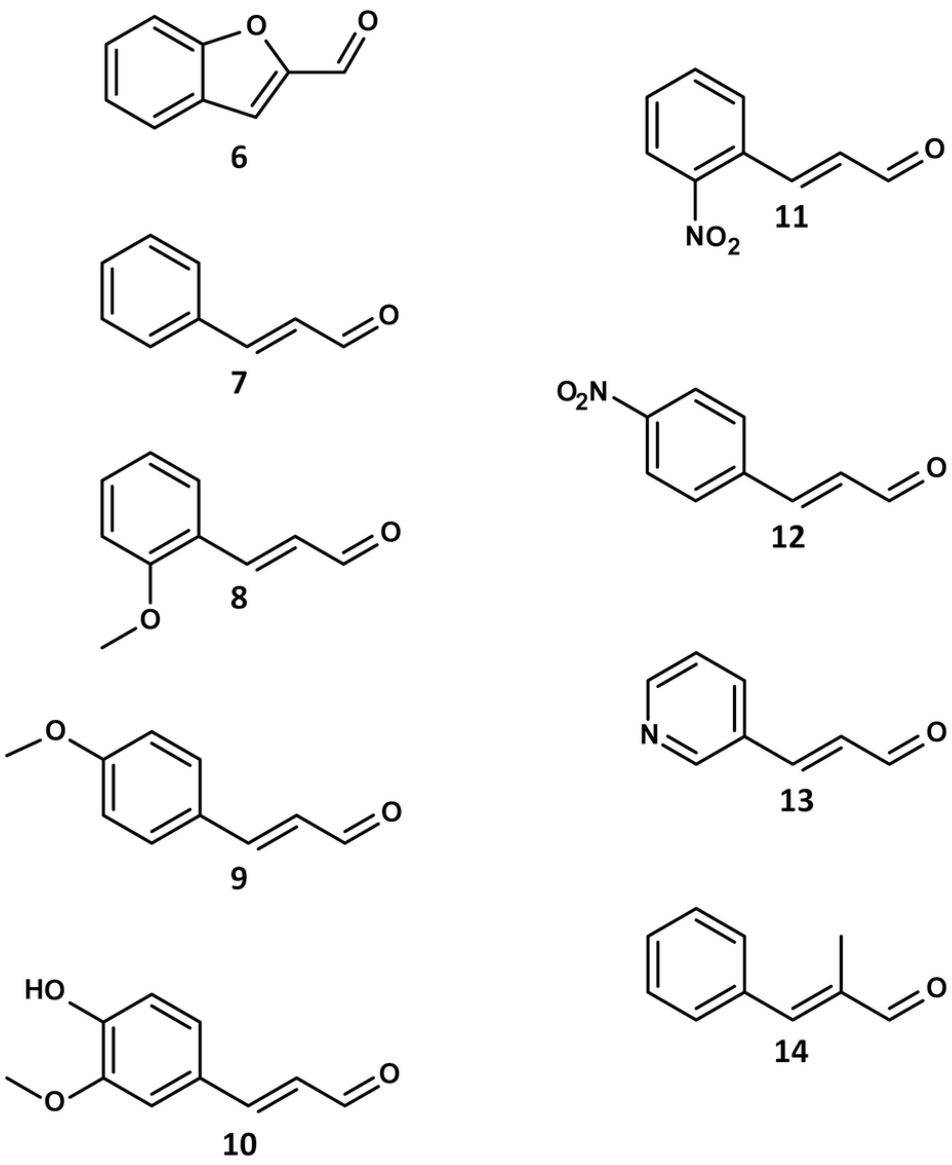

Scheme 2. Aldehyde substrates tested in steady state activity assays with SbAD.

82x98mm (300 x 300 DPI)

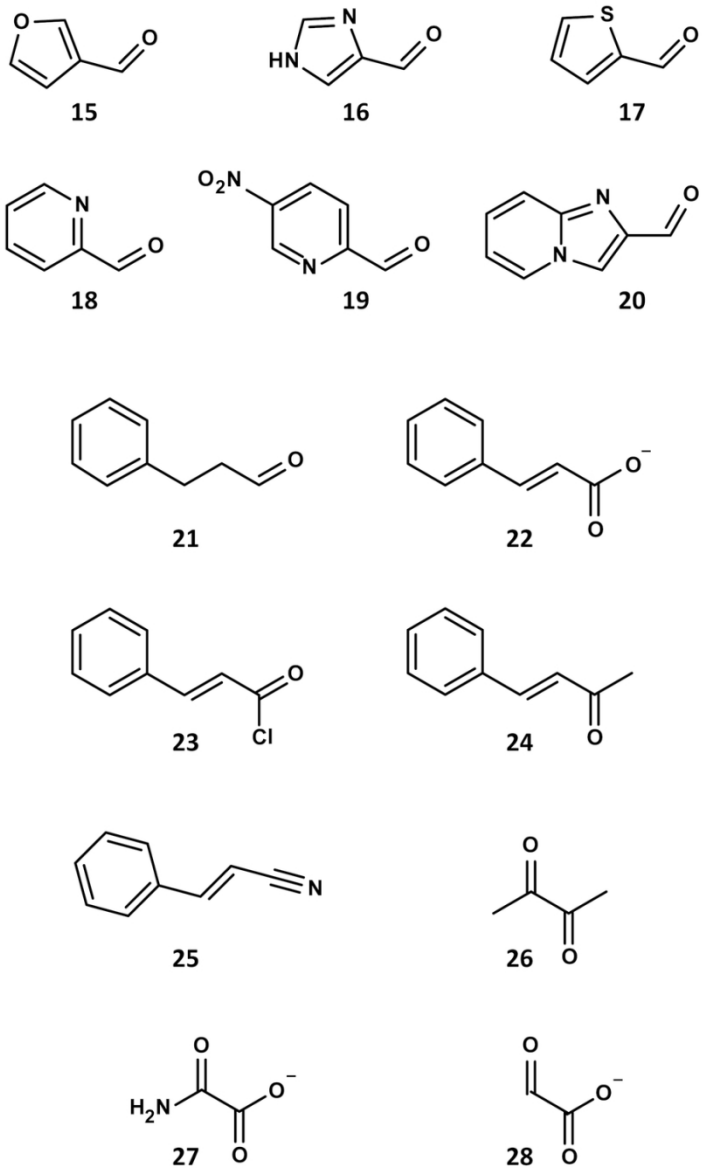

Scheme 3. Aldehydes tested for activity in the SbAD-catalyzed aldol condensation reaction and found not to be substrates.

82x133mm (300 x 300 DPI)

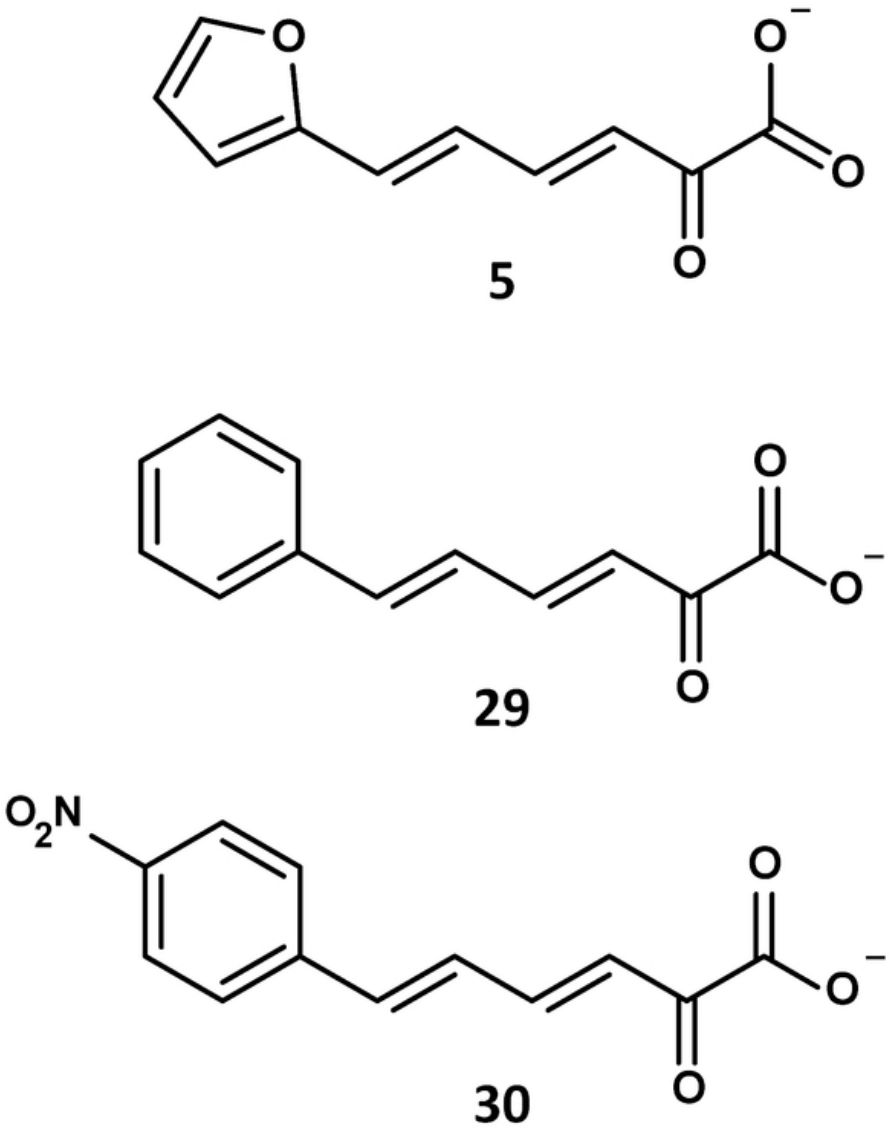

Scheme 4. Dieneone compounds tested for activity in the SbAD-catalyzed retro-aldol cleavage reaction.

50x66mm (300 x 300 DPI)

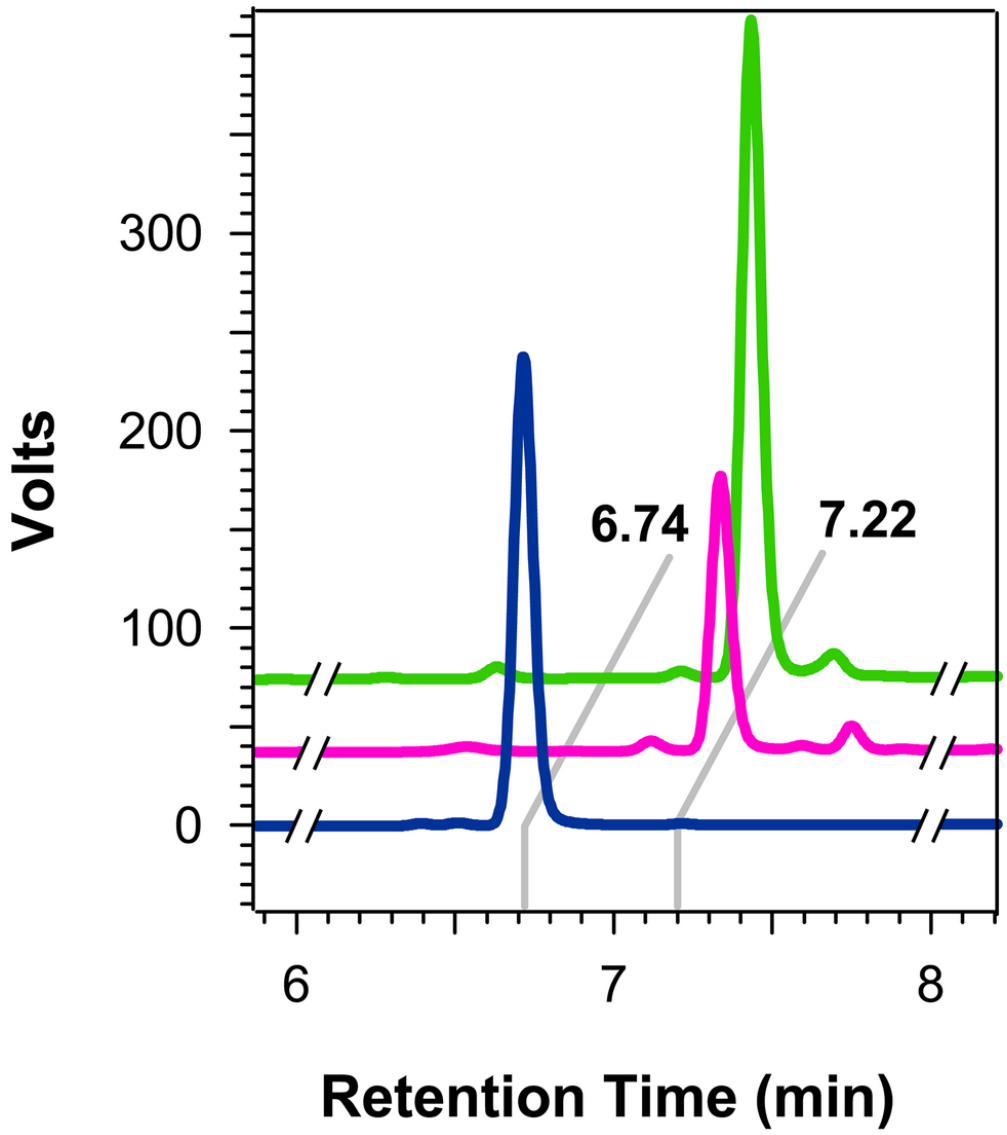

Figure 2. Reversed phase HPLC chromatograms showing SbAD-catalyzed aldol condensation of pyruvate and 12. The authentic 12 standard (blue trace) elutes at 6.74 min, while authentic 30 elutes at 7.22 min (magenta trace). Standards were 200 μM in 100 mM MOPS pH 7.0. A reaction containing 10 μM SbAD, 100 mM pyruvate, and 200 μM 12, was prepared in 100 mM MOPS pH 7.0 (green trace). After standing at RT for 20h, only the condensation product 30 is detectable.

82x93mm (300 x 300 DPI)

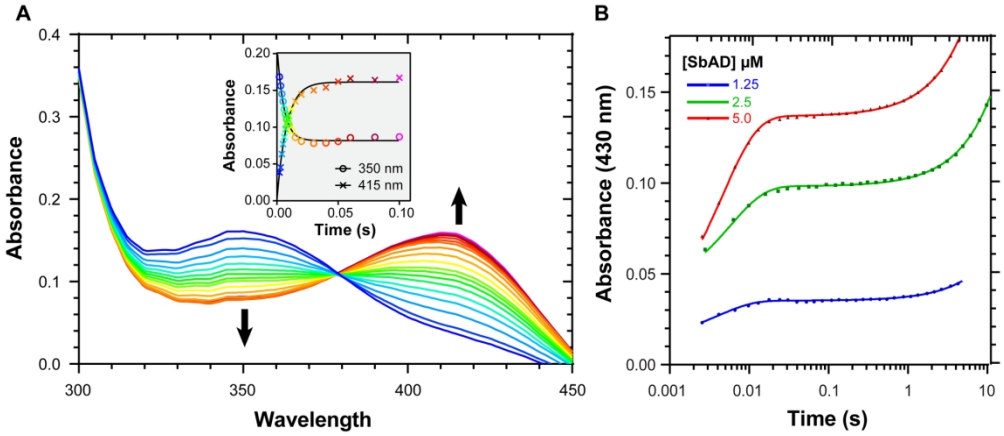

Figure 3. Pre-steady state kinetics of SbAD-catalyzed retro-aldol cleavage of 30. When wild-type SbAD was mixed with 30 (100 µM and 20 µM, respectively, after mixing) the absorbance at 350 nm, due to 30, decreased and the absorbance at 415 nm increased (A). The data begin at 2 ms (blue) and end at 100 ms (magenta). The inset shows the time course of these spectral changes. Burst kinetics were observed when limiting amounts of wild-type SbAD (1.25 µM [blue], 2.5 µM [green], or 5.0 µM [red]) were mixed with saturating amounts of pyruvate (200 mM) and cinnamaldehyde (2.5 mM) (B). Only every 20th data point is plotted to better show the non-linear fits. All reactions were performed in 100 mM Bis-TRIS pH 6.5.

177x76mm (300 x 300 DPI)

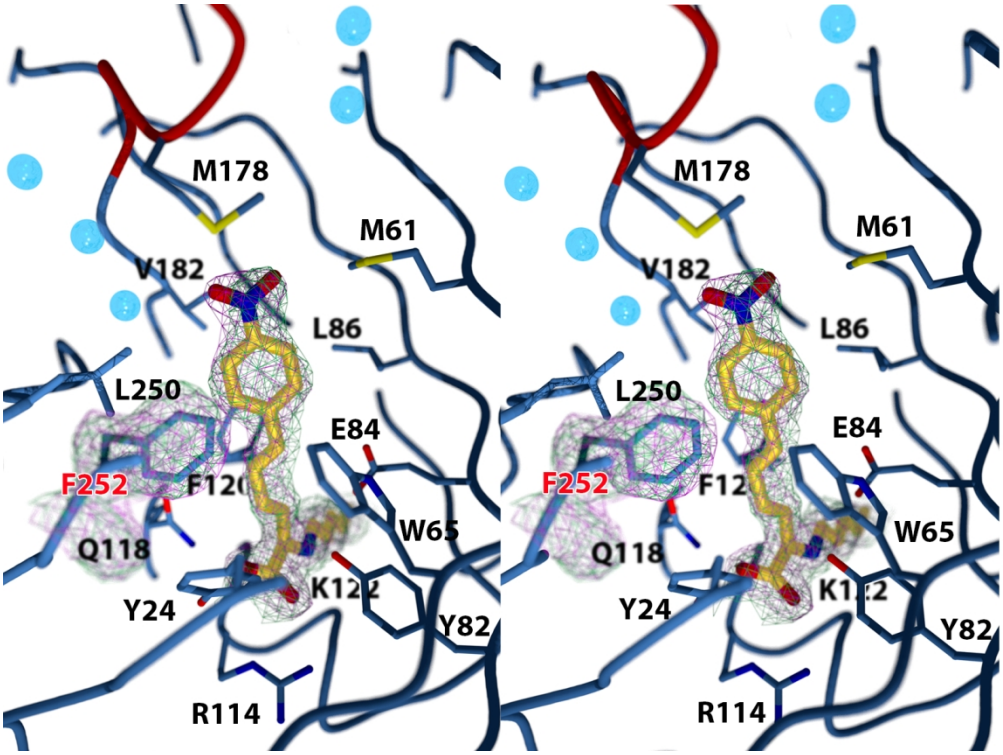

Figure 4. Crystal structure of SbADY252F with the 30-derived intermediate bound in the active site. 2Fo-Fc electron density is in magenta and simulated annealing omit electron density is in green. Both are contoured at 1.2σ. Selected water molecules (blue spheres) are shown to highlight the paths to the bulk solvent on either side of the active site loop (red).

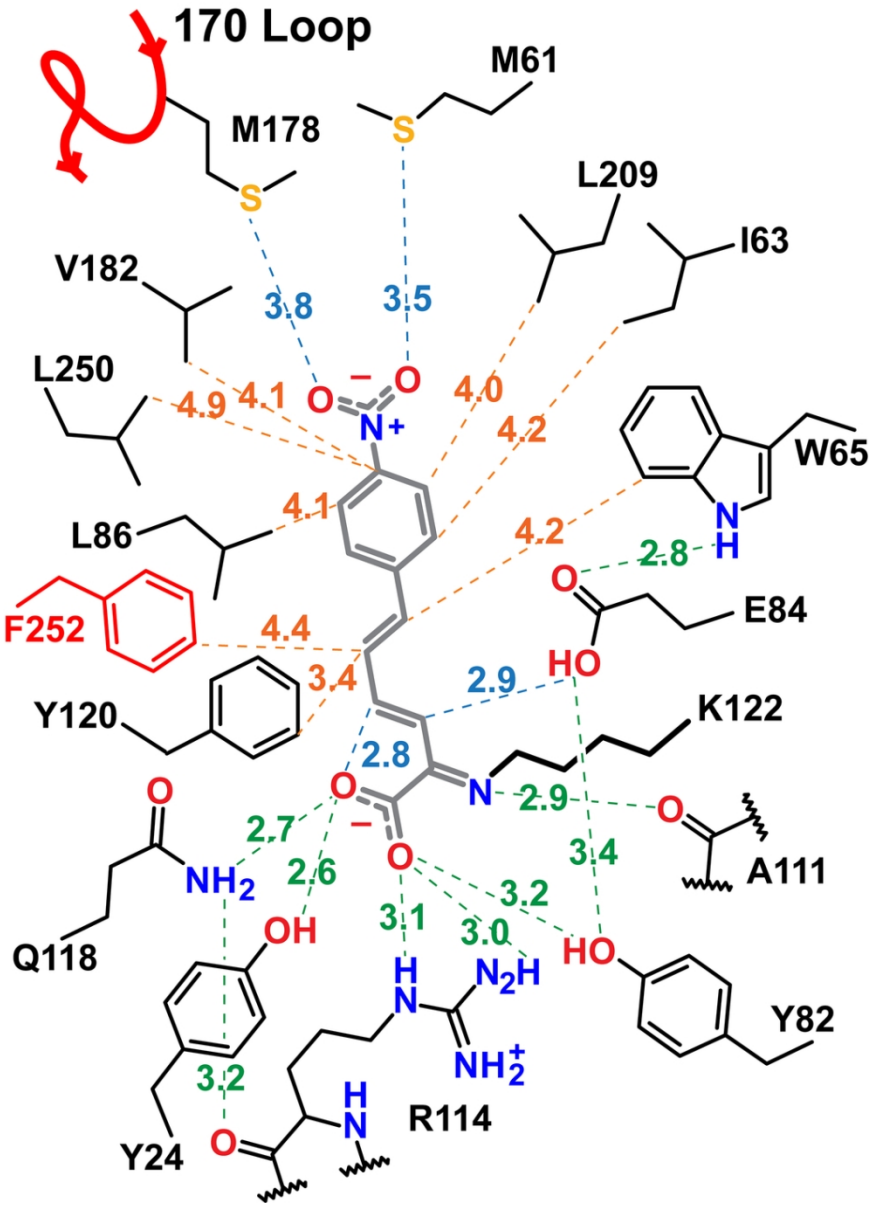

Figure 5. Interactions between the 30-derived intermediate and the SbADY252F active site. Hydrogen bonding interactions are shown as green, dotted lines with associated donor-acceptor distances in Å. Orange, dotted lines represent hydrophobic contacts, and blue, dotted lines are informational and do not represent any type of interaction.

88x123mm (300 x 300 DPI)

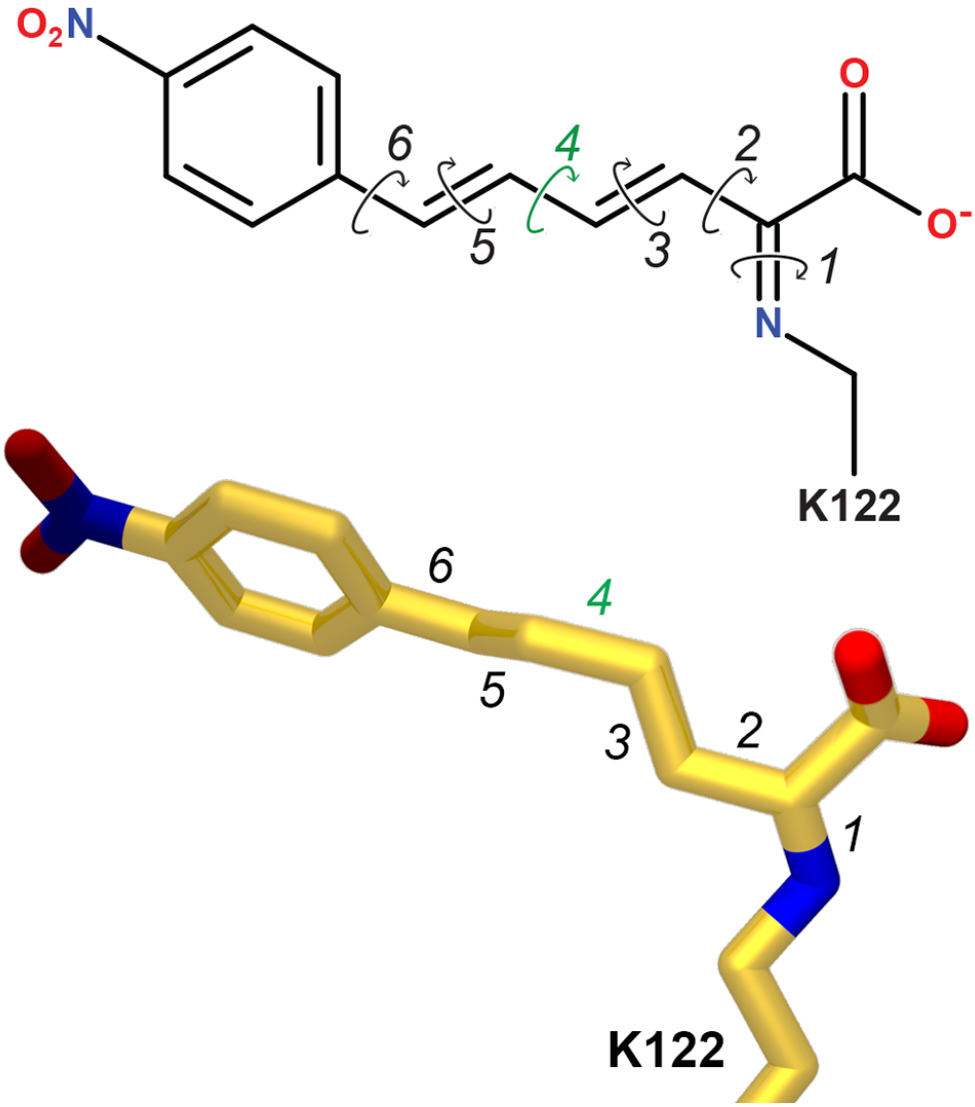

Figure 6. The proposed intermediate based on the crystal structure. The dihedral angles corresponding to numbers 1-6 are listed in Table 8.

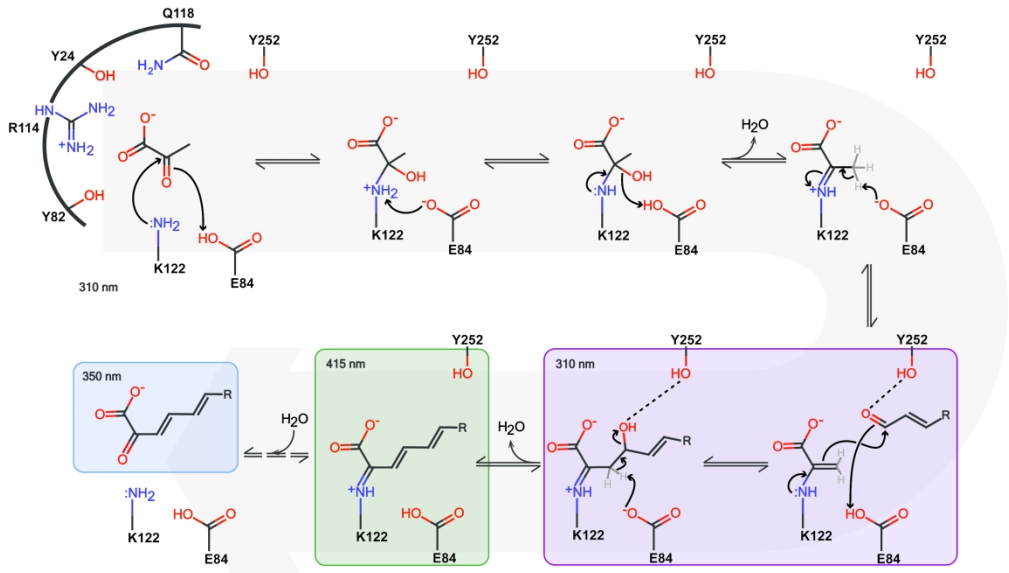

Figure 7. The proposed mechanism of SbAD. R represents phenyl (i.e. 29) or p-nitrophenyl (i.e. 30).